ChIP assays detected higher levels of trimethylated H3K27 and EZH2 occupancy in cells showing lower expression levels of miR-31 (Figure S4H). Furthermore, knockdown of EZH2 or SUZ12 restored miR-31 transcription in MDA-MB-453 and MCF7 cells (Figures 5F and 5G; Figure S4K, respectively), which are consistent with the results obtained with ATL cells. These results indicate a link between Polycomb-mediated epigenetic regulation and miR-31 transcription in ATL and breast cancer cell lines.

Polycomb Group Regulates NF-κB Pathway by Controlling miR-31 Expression

Based on our findings, we considered an aspect of the biological communication between epigenetic silencing and the NF-κB pathway through miR-31 regulation. The microarray data sets showed positive correlations between PRC2 components and miR-31 target gene, *NIK* expression (Figure 6A). The results also suggested that these factors tend to show higher levels in the aggressive subtype (acute type) than in the indolent subtypes (chronic and smoldering types), implying that these genes may play important roles in the clinical phenotype and prognosis of ATL. To examine this notion, we performed PRC2 knockdown in ATL cell lines. Western blots of these cells demonstrated decreased levels of NIK, p52, and phospho-IκBα (Figure 6B; Figure S5A), suggesting suppression of both canonical and noncanonical NF-κB cascade and activity (Figure 6C; Figures S5B and S5C). These results are consistent with those of miR-31 overexpression (Figures 3C–3F). Then, we tested whether exogenous manipulation of miR-31 could restore the effect of PRC2 loss. Anti-miR-31 treatment rescued impaired NF-κB activity in PRC2-disrupted cells (Figure 6D). On the other hand, overexpression of EZH2 induced NF-κB activation, which was partially canceled by the introduction of miR-31 precursor (Figure 6E; Figure S5D). These results suggest that Polycomb-mediated miR-31 suppression leads to NF-κB activation. Indeed, knockdown of the PRC2 complex led to reduced levels of cell proliferation and greater sensitivity to serum deprivation in ATL cells (Figure 6F; Figure S5E). In addition, PRC2 disruption showed a reduction in cell migration (Figure S5F).

To gain further insight into this general network, we studied the functions of miR-31 and the PRC2 complex in breast cancer cell lines. NF-κB activity was downregulated by knockdown of PRC2 components in MDA-MB-453 cells (Figure 6G; Figures S5G and S5H), although no significant differences were observed in cell proliferation (data not shown). Repression of NF-κB activity induced by knockdown of PRC2 components was partially restored by treatment with a miR-31 inhibitor, suggesting that PRC2 knockdown-mediated relief of NF-κB repression is at least a part of the result of the miR-31 induction. In addition, knockdown of PRC2 components resulted in a reduced level of receptor-initiated accumulation of NIK in B cells (Figure 6H). Our findings indicate a common molecular mechanism comprising Polycomb-mediated epigenetic regulation, miR-31 expression and the NF-κB signaling pathway.

Regulation of NF-κB by Polycomb family may in turn control the cellular apoptosis responses. We found that lentivirus-mediated EZH2 knockdown led to increased apoptotic sensitivity in TL-Om1 cells (Figure 6I). Additional expression of NIK inhibited the cell death induced by EZH2 knockdown, suggesting the reciprocal relationship between Polycomb and NF-κB cascades. By using primary tumor cells from patient, we tested the killing effect induced by miR-31, NIK knockdown, and EZH2 knockdown (Figure 6J; Figures S5I and S5J). All tested samples showed strong death response, demonstrating that survival of ATL cells was closely associated with miR-31, NIK, and EZH2, all of which show deregulated expression in ATL cells.

By qRT-PCR we finally examined the expression levels of some genes involved in the noncanonical NF-κB pathway. As shown in Figure 6K, the results clearly demonstrated higher expression levels of positive regulators such as *NIK*, *CD40,* and *LTBR*, and lower expression levels of the negative regulators such as *BIRC2/3* (cIAP1/2), which are involved in proteasomal degradation of NIK (Zarnegar et al., 2008a). These observations are in line with a previous report on Multiple Myeloma cells (Annunziata et al., 2007). In addition to these data, we obtained convincing evidence for a molecular aspect of NIK accumulation in ATL cells. Polycomb-dependent epigenetic gene silencing may be associated with miR-31 loss, followed by NF-κB activation and other signaling pathways (Figure 7).

DISCUSSION

Constitutive activation of NF-κB contributes to abnormal proliferation and inhibition of apoptotic cell death in cancer cells,

Figure 4. Genetic and Epigenetic Abnormalities Cause miR-31 Loss in ATL Cells

(A) Genomic loss of chromosome 9p21.3 in primary ATL cells. Copy number analyses revealed tumor-associated deletion of miR-31 region (21/168) and *CDKN2* region (46/168). Recurrent genetic changes are depicted by horizontal lines based on CNAG output of the SNP array analysis.

(B) miR-31 expression in various sample sets. Expression levels were evaluated by real-time PCR.

Loss, samples with genomic loss of the miR-31 region; (–) samples without genomic loss of the miR-31 region.

(C) PCR-based miR-31 quantifications in primary ATL samples. ATL samples without genetic loss in miR-31 region (n = 9, Figure S3B), and normal CD4+ T cells (n = 7) were tested. p values (ATL versus normal) are shown.

(D) YY1 binding motif cluster around transcriptional start site (TSS) of miR-31 region. Arrows represent positions of the motifs. Regions of PCR amplification for ChIP assay are shown.

(E) Repression-associated histone methylation in miR-31 region determined by ChIP assay (n = 3, mean ± SD). The results of relative enrichment against input control are presented and distance from miR-31 TSS is described. *MYT1* and *GAPDH* promoters are as positive or negative controls, respectively.

(F–I) YY1-dependent EZH2 occupancy in miR-31 locus. (F) YY1 knockdown in TL-Om1 cells. qRT-PCR (left, n = 3, mean ± SD) and western blotting (right) showed decreased YY1 level. (G) YY1 knockdown led to both primary and mature miR-31 restoration in TL-Om1 cells (n = 3, mean ± SD). (H) YY1 occupancy in miR-31 region analyzed by ChIP (n = 3, mean ± SD). YY1 occupancy in miR-31 locus was reduced by YY1 knockdown. (I) EZH2 occupancy in miR-31 region analyzed by ChIP (n = 3, mean ± SD). YY1 knockdown inhibited EZH2 recruitment in miR-31 region.

(J) Aberrant accumulation of repression-associated histone methylations widely in miR-31 region of primary ATL cells. PBMCs freshly isolated from ATL patients (n = 6) were analyzed by ChIP assay. PBMC from healthy adults were used for normal controls. See also Figure S3.

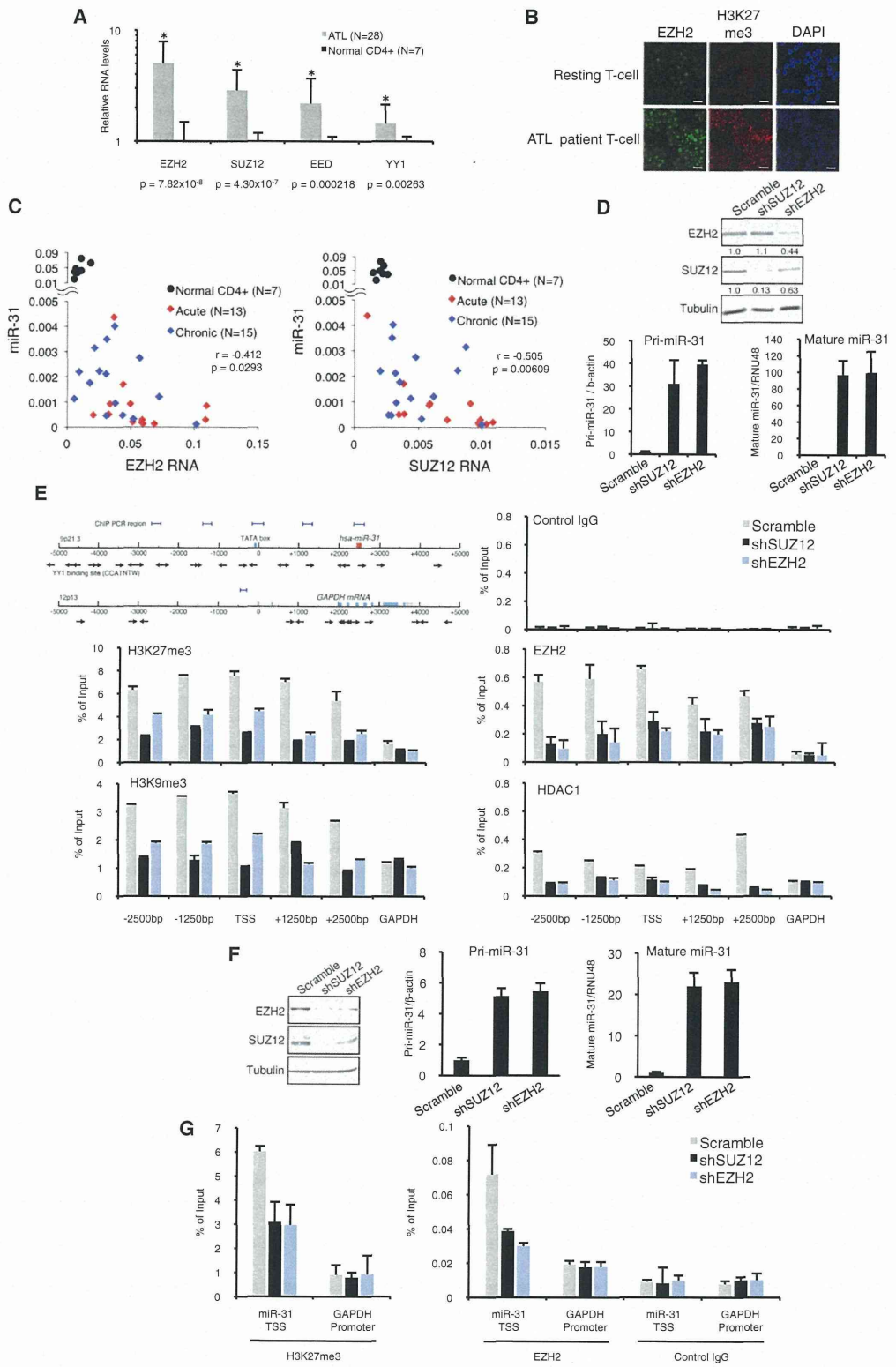
A
Relative RNA levels
ATL (N=28)
Normal CD4+ (N=7)
EZH2
SUZ12
EED
YY1
p = 7.82x10-8
p = 4.30x10-7
p = 0.000218
p = 0.00263
B
H3K27 me3
EZH2
DAPI
Resting T-cell
ATL patient T-cell
C
miR-31
Normal CD4+ (N=7)
Acute (N=13)
Chronic (N=15)
r = -0.412
p = 0.0293
EZH2 RNA
r = -0.505
p = 0.00609
SUZ12 RNA
D
Scramble
shSUZ12
shEZH2
EZH2
SUZ12
Tubulin
Pri-miR-31
Pri-miR-31 / b-actin
Mature miR-31
Mature miR-31/RNU48
E
ChIP PCR region
TATA box
hsa-miR-31
YY1 binding site (CCATNTW)
GAPDH mRNA
Control IgG
H3K27me3
EZH2
H3K9me3
HDAC1
% of Input
-2500bp
-1250bp
TSS
+1250bp
+2500bp
GAPDH
F
Scramble
shSUZ12
shEZH2
EZH2
SUZ12
Tubulin
Pri-miR-31
Pri-miR-31/β-actin
Mature miR-31
Mature miR-31/RNU48
G
% of Input
miR-31 TSS
GAPDH Promoter
H3K27me3
EZH2
Control IgG
Scramble
shSUZ12
shEZH2

including ATL, diffuse large B cell lymphoma (DLBCL), Hodgkin lymphoma, breast cancer, prostate cancer and others (Prasad et al., 2010). NF-κB is also essential for various cell functions, including inflammation, innate immunity, and lymphocytic development (Hayden and Ghosh, 2008). Identification of NF-κB determinants will lead to marked progress in understanding molecular pathology.

Our global analyses demonstrated an interesting miRNA expression signature as well as an aberrant mRNA expression profile, which may be associated with leukemogenesis in the primary ATL cells (Figures 1 and 6A). We revealed downregulation of tumor-suppressive miRNA including Let-7 family, miR-125b, and miR-146b, which can contribute to aberrant tumor cell signaling. Recent studies have suggested unique expression profiles of miRNAs in ATL (Yeung et al., 2008; Bellon et al., 2009), but loss of miR-31 has not been focused. Cellular amount of miRNAs may be susceptible to various environments such as transcriptional activity, maturation processing, and also epigenetic regulation. The end results appear to be affected by methodology employed and conditions and types of samples used. Our integrated expression profiling of primary ATL cells are based on a significantly larger number of samples and fruitfully provides intriguing information that may be useful in improving the understanding of T cell biology as well as in the identification of biomarkers for diagnosis.

Pleiotropy of miR-31 was first reported by Valastyan et al. (2009). The authors elegantly demonstrated the function of miR-31 in vivo and also identified several target genes that contribute to cell migration and invasiveness. In the present study, we focused on the functional significance of miR-31 in the regulation of NF-κB signaling that contributes to tumor cell survival.

Overexpression of NIK acts as an oncogenic driver in various cancers. In the present study, NIK was identified as a miR-31 target based on several lines of evidence. First, luciferase-3′ UTR reporter assay showed that *NIK* 3′ UTR sequence has a role for negative regulation (Figure S1B). By combining a specific inhibitor and mutations in miR-31-binding site, we demonstrated that miR-31 recognizes and negatively regulates the *NIK* 3′ UTR (Figures 2A and 2D). Second, by introducing a miR-31 precursor or inhibitor, we showed that amount of miR-31 inversely correlates with levels of NIK expression and downstream signaling (Figures 2E–2K). Third, genetic evidence indicated strong base pairing and biological conservation (Bartel, 2009) (Figures S1L–S1O). Our experimental approach illustrated that mmu-miR-31 regulates mouse *Map3k14* gene. Fourth, individual assessments using gene expression data clearly revealed an inverse correlation between the expression levels of miR-31 and *NIK* (Figure 3A). Collectively, we provide definitive evidence for the notion that miR-31 negatively regulates NIK expression and activity.

It is well known that the NIK level directly regulates NF-κB activity in various cell types (Thu and Richmond, 2010). We experimentally showed that miR-31 regulates noncanonical NF-κB activation stimulated by BAFF and CD40L, both of which are major B cell activating cytokines. Since signals from receptors are essential for the development and activity of B cells, the negative role of miR-31 in cytokines-induced NIK accumulation appears to be widely important in the noncanonical regulation of NF-κB in B cells and other cell types (Figures 2H–2K). Again, our findings revealed the role of NIK in the regulation of canonical NF-κB pathway. Strict regulation of NIK appears to be closely associated with the fate of lymphocytes.

The level of miR-31 was drastically suppressed in all tested primary ATL cells, and its magnitude is greater than that which has been reported in other cancers. Our results demonstrated a profound downregulation of miR-31 (fold change, 0.00403; Figure 1B) in all ATL cases, suggesting that miR-31 loss is a prerequisite for ATL development. Restoration of miR-31-repressed NF-κB activity in ATL cells, resulting in impairment of the proliferative index and apoptosis resistance (Figure 3). Furthermore, our results demonstrate that inhibition of NF-κB promotes tumor cell death in cell lines and also primary tumor cells from ATL patients (Figures 3 and 6), which are consistent with our previous observation (Watanabe et al., 2005). Since it is highly possible that miR-31 and relevant factors are pivotal in cancers, their expressions would have a great importance in view of biomarkers for the aberrant signaling and clinical outcomes.

By studying clinical samples and in vitro and ex vivo models, we obtained several biologically interesting results. First, we identified the Polycomb protein complex as a strong suppressor of miR-31. Generally, the Polycomb group constitutes a multimeric complex that negatively controls a large number of genes involved in cellular development, reproduction, and stemness (Sparmann and van Lohuizen et al., 2006). However, the key molecules involved in cancer development, progression, and prognosis are not yet fully understood. In breast and prostate cancers, oncogenic functions of EZH2 and NF-κB activation were reported independently (Kleer et al., 2003; Varambally et al., 2002; Suh and Rabson, 2004). Interestingly, these tumors show low miR-31 levels (Valastyan et al., 2009; Schaefer et al., 2010). Recently, Min et al. (2010) reported that EZH2 activates NF-κB by silencing the DAB2IP gene in prostate cancer cells.

Figure 5. Amount of PRC2 Components Epigenetically Links to miR-31 Expression in T Cells and Epithelial Cells

(A) Overexpression of PRC2 components in primary ATL cells measured by qRT-PCR (ATL, n = 28; normal, n = 7; mean ± SD). These results were supported by the data of gene expression microarray (Table S3).

(B) Escalation of EZH2 protein and trimethylated H3K27 levels in primary ATL cells illustrated by immunocytostaining (n = 4, a representative result is shown). Resting T cells were as normal control. Scale bars = 20 μm.

(C) Statistical correlation among the levels of miR-31, *EZH2*, and *SUZ12* in individual ATL samples. Correlation coefficients within ATL samples are shown in the graphs.

(D and E) Loss of PCR2 function causes chromatin rearrangement and miR-31 upregulation. (D) TL-Om1 cells expressing shSUZ12, shEZH2, and scrambled RNA were established by retroviral vector. The levels of EZH2, SUZ12, *Pri-miR-31*, and mature miR-31 were measured by western blotting and qRT-PCR (n = 3, mean ± SD). (E) Results of ChIP assays with indicated antibodies (n = 3, mean ± SD). Amounts of immunoprecipitated DNA were analyzed by region-specific PCR. *GAPDH* promoter served as a region control.

(F and G) Knockdown of Polycomb family proteins in MDA-MB-453 cells. (F) EZH2 and SUZ12 are shown by western blot. miR-31 level was examined by qRT-PCR (n = 3, mean ± SD). (G) Histone methylation and EZH2 occupancy evaluated by ChIP assay (n = 3, mean ± SD). See also Table S3 and Figure S4.

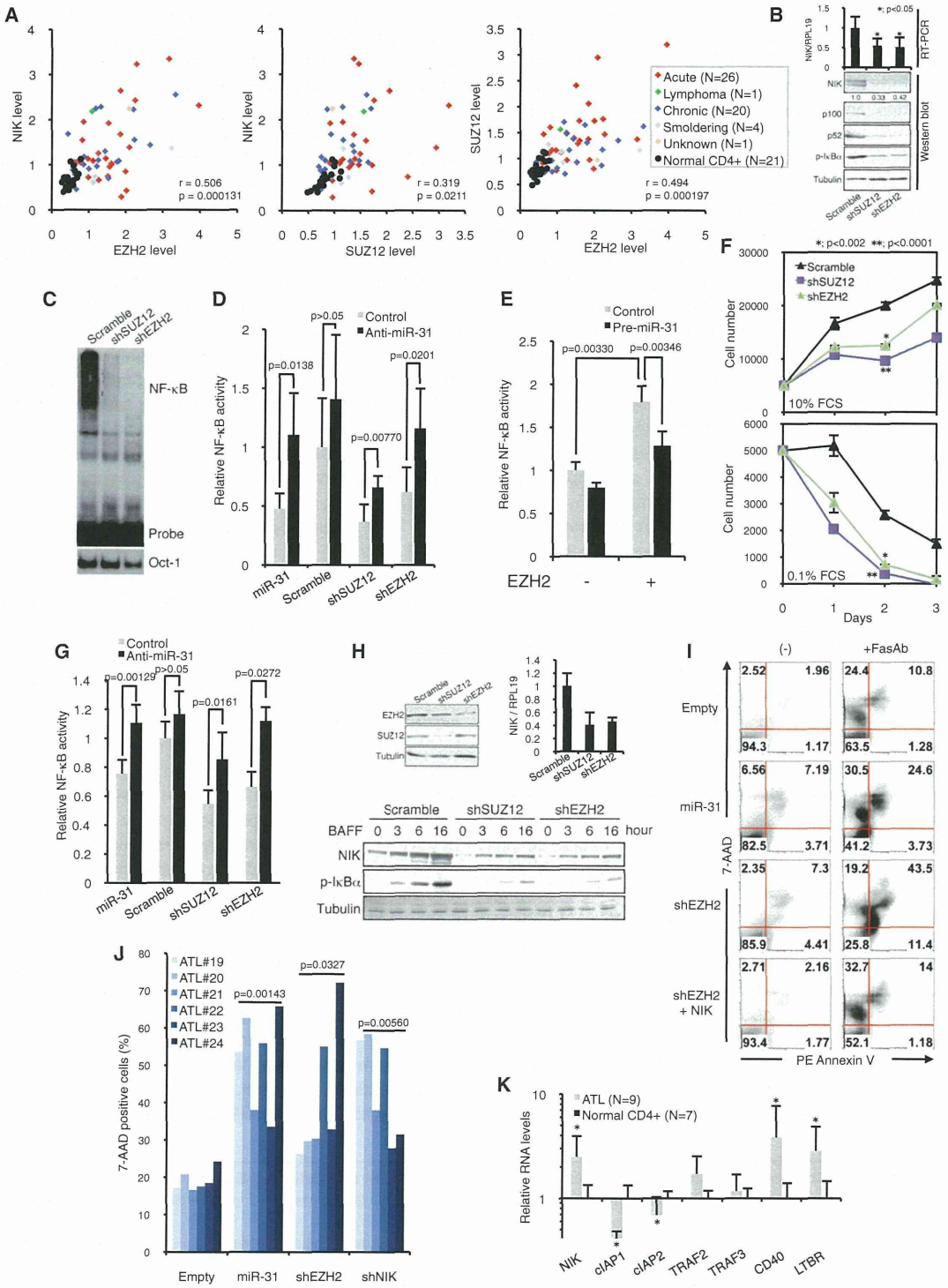

Figure 6. Epigenetic Change Driven by Polycomb Group Mediates NF-κB Signaling through miR-31 Regulation

(A) Reciprocal relationship of mRNA expression between *NIK* and Polycomb group in primary samples. Pearson's correlation coefficients among ATL samples are shown.

(B) PRC2 knockdown negatively affects NF-κB signaling in TL-Om1 cells. After establishment of PRC2 knockdown, the levels of *NIK* RNA (n = 4, mean ± SD) and proteins of NIK, p52/p100, and phospho-IκBα were examined.

(C) Downregulation of NF-κB activity in PRC2-disrupted cells detected by EMSA.

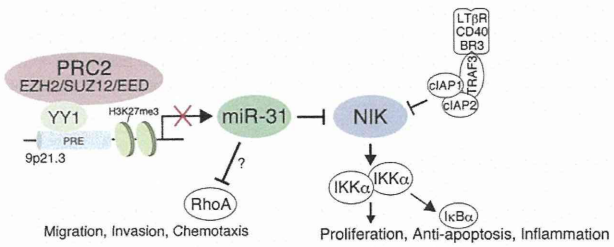

Figure 7. Proposed Model for ATL and Other Tumor Cells
Polycomb repressive factors are linked to NIK-dependent NF-κB activation via miR-31 regulation.

In the present study, we found that the Polycomb group regulates miR-31 expression and that elevated expression of EZH2 leads to NF-κB activation via NIK-miR-31 regulation in ATL and breast cancer cells (Figure 6). We also showed that restoration of miR-31 partially impaired Polycomb-mediated NF-κB operation (Figures 6D, 6E, and 6G), suggesting that miR-31 is involved in this relationship. Furthermore, a connection between NIK and PRC2 was observed in B cells (Figure 6H). Polycomb group proteins are essential in lymphocyte development and activation (Su et al., 2003, 2005). Further, given the NF-κB is a pivotal transcription regulator in normal and oncogenic functions, practical participations of epigenetic regulators and miR-31 in NF-κB signaling will increase our understanding of the molecular mechanisms of T cell functions. For generalization of the molecular axis in other cancers and normal cells, further study will be needed.

Second, YY1 is a recruiter of PRC2 to the miR-31 region. In humans, the Polycomb response element (PRE) has not been precisely identified. A good candidate for a mammalian recruiter of PRC2 is YY1, the homolog of *D. melanogaster* PHO (Simon and Kingston, 2009). We found an assembly of the YY1 binding motif in the miR-31 locus and demonstrated that YY1 knockdown dislodged EZH2 in this region (Figure 4I), which supports previous findings (Caretti et al., 2004). The detailed mechanism by which YY1 mediates recruitment of the Polycomb family may be important in the context of epigenetic regulation of orchestrated gene expression and T cell functions.

Third, Polycomb family proteins can control miRNA expression in an epigenetic fashion. The amount of PRC2 factors strongly influenced the degree of suppression of miR-31 expression (Figure 5). We speculate that, in addition to controlling the transcription, the Polycomb group can modulate translation via miRNA regulation. Furthermore, miR-101 and miR-26a are known to regulate EZH2 expression (Sander et al., 2008; Varambally et al., 2008), which is supported by our observation (Figure S4C). This signaling circuit will permit multiple gene regulation. Whereas genetic loss at the miR-31 locus is observed in some cases of ATL (Figure 4A), no genetic deletion in the miR-101-1 or miR-101-2 region was detected in ATL, which is not consistent with a previous finding in prostate cancer. Our results also suggested putative association between Let-7 family and EZH2 (Figure S4). Aberrant downregulations of these miRNAs in the primary ATL cells will be the next important questions to be addressed in efforts to improve understanding of the oncogenic signaling network.

By collaborative profiling of miRNA and mRNA expression, we identified a notable relationship between ATL subtypes and a gene cluster that contains miR-31, NIK, EZH2, and SUZ12. This finding suggests that an aberrant gene expression pattern correlates with the malignant phenotype, and this provides important clues about clinical manifestations and may help identify therapeutic targets against ATL cells (Figure 6A). Although HDAC inhibitors did not show effective responses (Figures S4I and S4J), emerging epigenetic drug such an EZH2 inhibitor (Fiskus et al., 2009) may pave a pathway leading to cures for various malignancies that involve constitutive activation of NF-κB.

In summary, we show that genetic and epigenetic loss of miR-31 is responsible for oncogenic NF-κB activation and malignant phenotypes in ATL. This provides evidence for the idea that miR-31 is an important tumor suppressor. An emerging pathway involving an epigenetic process, miR-31, and NF-κB will provide a conceptual advance in epigenetic reprogramming, inflammatory signaling, and oncogenic addiction.

EXPERIMENTAL PROCEDURES

Cell Lines and Primary ATL Cells

The primary peripheral blood mononuclear cells (PBMCs) from ATL patients and healthy volunteers used in the present work were a part of those collected with an informed consent as a collaborative project of the Joint Study on Prognostic Factors of ATL Development (JSPFAD). The project was approved by the Institute of Medical Sciences, the University of Tokyo (IMSUT) Human Genome Research Ethics Committee. Additional ATL clinical samples for copy number analysis were provided by Drs. Y. Yamada, Nagasaki University,

(D) NF-κB activity evaluated by reporter assays in the presence or absence of miR-31 inhibitor (n = 5, mean ± SD). Anti-miR-31 treatment partially rescued the NF-κB activity in PRC2 knockdowned TL-Om1 cells.
(E) Overexpressed EZH2 activates NF-κB via miR-31. Jurkat cells were transfected with an EZH2 plasmid together with miR-31 precursor or control RNA (n = 5, mean ± SD).
(F) PRC2 dysfunction changes TL-Om1 cell proliferation and response to serum starvation. Under conditions of 10% or 0.1% of FCS, cell growth curves were examined (n = 3, mean ± SD). PRC2 downregulation decreased cell growth with statistical significance.
(G) NF-κB activity in PRC2-knockdowned MDA-MB-453 cells in the presence or absence of miR-31 inhibitor were examined (n = 5, mean ± SD).
(H) PRC2 disruption inhibits BAFF-dependent NIK accumulation and IκBα phosphorylation in BJAB cells.
(I) Apoptotic cell death induced by lentivirus-mediated EZH2 knockdown in TL-Om1. Venus-positive populations were analyzed by Annexin V/7-AAD stainings (n = 3) and representative of FACS data are shown.
(J) Summary of primary tumor cell death. Lentivirus-based miR-31 expression, NIK knockdown, and EZH2 knockdown showed killing effects in six primary ATL samples. Statistical significances are shown in the graph. Results of FACS and qRT-PCR are shown in Figures S5I and S5J.
(K) Expression levels of genes involved in noncanonical NF-κB pathway in primary ATL cells (ATL, n = 9; normal, n = 7; mean ± SD). Relative expression levels were tested by qRT-PCR (*$p < 0.05$). See also Figure S5.

and K. Ohshima, Kurume University, where the projects were approved by the Research Ethics Committees of Nagasaki University and Kurume University, respectively. PBMC were isolated by Ficoll separation. ATL cells, primary lymphocytes, and all T cell lines were maintained in RPMI1640 supplemented with 10% of FCS and antibiotics. Clinical information of ATL samples is provided in Table S1.

Expression Analyses

Clinical samples for microarrays were collected by a collaborative study group, JSPFAD (Iwanaga et al., 2010). Gene expression microarray was used 4x44K Whole Human Genome Oligo Microarray (Agilent Technologies) and miRNA microarray was used Human miRNA microarray kit v2 (Agilent Technologies), respectively. Quantitative RT-PCR was performed with SYBRGreen (TAKARA). Mature miRNA assays were purchased from Applied Biosystems.

Copy Number Analyses

Genomic DNA from ATL patients was provided from the material bank of JSPFAD, Nagasaki University, and Kurume University, and was analyzed by Affymetrix GeneChip Human Mapping 250K Nsp Array (Affymetrix). Obtained data were analyzed by CNAG/AsCNAR program (Chen et al., 2008).

Oligonucleotides, Plasmids, and Retrovirus Vectors

All RT-PCR primers and oligonucleotides are described in Supplemental Experimental Procedures. miRNA precursor and inhibitor were from Applied Biosystems. Transfection of small RNA and other plasmid DNA were performed by Lipofectamine2000 (Invitrogen). For miRNA or shRNA expression, retroviral vectors (pSINsi-U6, TAKARA) were used.

3′ UTR-Conjugated miR-31 Reporter Assay

HeLa cells were cotransfected with 3′ UTR-inserted pMIR-REPORT firefly plasmid (Ambion), RSV-Renilla luciferase plasmid, and miRNA inhibitor. The cells were collected at 24 hr posttransfection, and Dual-luciferase reporter assay was performed (Promega).

Analysis of NF-κB Pathway

NF-κB activity was evaluated by EMSA and reporter assays as previously described (Horie et al., 2004). Antibodies for western blots are described in supplemental information. Cell proliferative assay was performed by Cell Counting Kit-8 (Dojindo).

Lentivirus Vectors and Apoptosis Analysis

A lentivirus vector (CS-H1-EVBsd) was provided from RIKEN, BRC, Japan. Lentivirus solution was produced by cotransfection with packaging plasmid (pCAG-HIVgp) and VSV-G- and Rev-expressing plasmid (pCMV-VSV-G-RSV-Rev) into 293FT cells. After infection of lentivirus, the apoptotic cell was evaluated by PE Annexin V / 7-AAD staining (BD PharMingen) and analyzed by FACS Calibur (Becton, Dickinson). Collected data were analyzed by FlowJo software (Tree Star).

ChIP Assay

ChIP assay was previously described (Yamagishi et al., 2009). Briefly, cells were crosslinked with 1% of formaldehyde, sonicated, and subjected to chromatin-conjugated IP using specific antibodies. Precipitated DNA was purified and analyzed by real-time PCR with specific primers (see Supplemental Experimental Procedures).

Computational Prediction

To identify miR-31 target genes, we integrated the output results of multiple prediction programs; TargetScan, PicTar, miRanda, and PITA. RNAhybrid was for secondary structure of miRNA-3′ UTR hybrid. TSSG program was for TATA box and TSS predictions. DNA methylation site was predicted by CpG island Searcher.

Statistical Analyses

Data were analyzed as follows: (1) Welch's t test for Gene Expression Microarray (p value cutoff at 10^{-6}) and miRNA Microarray (p value cutoff at 10^{-5}); (2) Pearson's correlation for two-dimensional hierarchical clustering analysis and individual assessment of microarray data sets; (3) two-tailed pared Student's t test with $p < 0.05$ considered statistically significant for in vitro cell lines and primary cells experiments, including luciferase assay, RT-PCR, ChIP assay, cell growth assay, and migration assay. Data are presented as mean ± SD.

ACCESSION NUMBERS

Coordinates have been deposited in Gene Expression Omnibus database with accession numbers, GSE31629 (miRNA microarray), GSE33615 (gene expression microarray), and GSE33602 (copy number analyses).

SUPPLEMENTAL INFORMATION

Supplemental Information includes three tables, five figures, and Supplemental Experimental Procedures and can be found with this article online at doi:10.1016/j.ccr.2011.12.015.

ACKNOWLEDGMENTS

We thank Dr. M. Iwanaga, Mr. M. Nakashima, and Ms. T. Akashi for support and maintenance of JSPFAD. We thank Drs. H. Miyoshi and A. Miyawaki for providing the Venus-encoding lentivirus vectors. We also thank Dr. R. Horie for experimental advices, and Drs. T. Kanno and T. Ishida for providing the MDA-MB-453. Grant support: Grants-in-Aid for Scientific Research from Ministry of Education, Culture, Sports, Science, and Technology of Japan to T.W. (No. 23390250) and by Grants-in-Aid from the Ministry of Health, Labour and Welfare to T.W. (H21-G-002 and H22-AIDS-I-002).

Received: November 3, 2010
Revised: August 12, 2011
Accepted: December 19, 2011
Published: January 17, 2012

REFERENCES

Annunziata, C.M., Davis, R.E., Demchenko, Y., Bellamy, W., Gabrea, A., Zhan, F., Lenz, G., Hanamura, I., Wright, G., Xiao, W., et al. (2007). Frequent engagement of the classical and alternative NF-kappaB pathways by diverse genetic abnormalities in multiple myeloma. Cancer Cell *12*, 115–130.

Bartel, D.P. (2009). MicroRNAs: target recognition and regulatory functions. Cell *136*, 215–233.

Bellon, M., Lepelletier, Y., Hermine, O., and Nicot, C. (2009). Deregulation of microRNA involved in hematopoiesis and the immune response in HTLV-I adult T-cell leukemia. Blood *113*, 4914–4917.

Caretti, G., Di Padova, M., Micales, B., Lyons, G.E., and Sartorelli, V. (2004). The Polycomb Ezh2 methyltransferase regulates muscle gene expression and skeletal muscle differentiation. Genes Dev. *18*, 2627–2638.

Chen, Y., Takita, J., Choi, Y.L., Kato, M., Ohira, M., Sanada, M., Wang, L., Soda, M., Kikuchi, A., Igarashi, T., et al. (2008). Oncogenic mutations of ALK kinase in neuroblastoma. Nature *455*, 971–974.

Davis, B.N., Hilyard, A.C., Lagna, G., and Hata, A. (2008). SMAD proteins control DROSHA-mediated microRNA maturation. Nature *454*, 56–61.

Fiskus, W., Wang, Y., Sreekumar, A., Buckley, K.M., Shi, H., Jillella, A., Ustun, C., Rao, R., Fernandez, P., Chen, J., et al. (2009). Combined epigenetic therapy with the histone methyltransferase EZH2 inhibitor 3-deazaneplanocin A and the histone deacetylase inhibitor panobinostat against human AML cells. Blood *114*, 2733–2743.

Hayden, M.S., and Ghosh, S. (2008). Shared principles in NF-kappaB signaling. Cell *132*, 344–362.

Hironaka, N., Mochida, K., Mori, N., Maeda, M., Yamamoto, N., and Yamaoka, S. (2004). Tax-independent constitutive IkappaB kinase activation in adult T-cell leukemia cells. Neoplasia *6*, 266–278.

Horie, R., Watanabe, M., Ishida, T., Koiwa, T., Aizawa, S., Itoh, K., Higashihara, M., Kadin, M.E., and Watanabe, T. (2004). The NPM-ALK oncoprotein

abrogates CD30 signaling and constitutive NF-kappaB activation in anaplastic large cell lymphoma. Cancer Cell *5*, 353–364.

Iwanaga, M., Watanabe, T., Utsunomiya, A., Okayama, A., Uchimaru, K., Koh, K.R., Ogata, M., Kikuchi, H., Sagara, Y., Uozumi, K., et al; Joint Study on Predisposing Factors of ATL Development investigators. (2010). Human T-cell leukemia virus type I (HTLV-1) proviral load and disease progression in asymptomatic HTLV-1 carriers: a nationwide prospective study in Japan. Blood *116*, 1211–1219.

Kleer, C.G., Cao, Q., Varambally, S., Shen, R., Ota, I., Tomlins, S.A., Ghosh, D., Sewalt, R.G., Otte, A.P., Hayes, D.F., et al. (2003). EZH2 is a marker of aggressive breast cancer and promotes neoplastic transformation of breast epithelial cells. Proc. Natl. Acad. Sci. USA *100*, 11606–11611.

Liao, G., Zhang, M., Harhaj, E.W., and Sun, S.C. (2004). Regulation of the NF-kappaB-inducing kinase by tumor necrosis factor receptor-associated factor 3-induced degradation. J. Biol. Chem. *279*, 26243–26250.

Malinin, N.L., Boldin, M.P., Kovalenko, A.V., and Wallach, D. (1997). MAP3K-related kinase involved in NF-kappaB induction by TNF, CD95 and IL-1. Nature *385*, 540–544.

Min, J., Zaslavsky, A., Fedele, G., McLaughlin, S.K., Reczek, E.E., De Raedt, T., Guney, I., Strochlic, D.E., Macconaill, L.E., Beroukhim, R., et al. (2010). An oncogene-tumor suppressor cascade drives metastatic prostate cancer by coordinately activating Ras and nuclear factor-kappaB. Nat. Med. *16*, 286–294.

Prasad, S., Ravindran, J., and Aggarwal, B.B. (2010). NF-kappaB and cancer: how intimate is this relationship. Mol. Cell. Biochem. *336*, 25–37.

Ramakrishnan, P., Wang, W., and Wallach, D. (2004). Receptor-specific signaling for both the alternative and the canonical NF-kappaB activation pathways by NF-kappaB-inducing kinase. Immunity *21*, 477–489.

Saitoh, Y., Yamamoto, N., Dewan, M.Z., Sugimoto, H., Martinez Bruyn, V.J., Iwasaki, Y., Matsubara, K., Qi, X., Saitoh, T., Imoto, I., et al. (2008). Overexpressed NF-kappaB-inducing kinase contributes to the tumorigenesis of adult T-cell leukemia and Hodgkin Reed-Sternberg cells. Blood *111*, 5118–5129.

Sander, S., Bullinger, L., Klapproth, K., Fiedler, K., Kestler, H.A., Barth, T.F., Möller, P., Stilgenbauer, S., Pollack, J.R., and Wirth, T. (2008). MYC stimulates EZH2 expression by repression of its negative regulator miR-26a. Blood *112*, 4202–4212.

Schaefer, A., Jung, M., Mollenkopf, H.J., Wagner, I., Stephan, C., Jentzmik, F., Miller, K., Lein, M., Kristiansen, G., and Jung, K. (2010). Diagnostic and prognostic implications of microRNA profiling in prostate carcinoma. Int. J. Cancer *126*, 1166–1176.

Simon, J.A., and Kingston, R.E. (2009). Mechanisms of polycomb gene silencing: knowns and unknowns. Nat. Rev. Mol. Cell Biol. *10*, 697–708.

Sparmann, A., and van Lohuizen, M. (2006). Polycomb silencers control cell fate, development and cancer. Nat. Rev. Cancer *6*, 846–856.

Su, I.H., Basavaraj, A., Krutchinsky, A.N., Hobert, O., Ullrich, A., Chait, B.T., and Tarakhovsky, A. (2003). Ezh2 controls B cell development through histone H3 methylation and Igh rearrangement. Nat. Immunol. *4*, 124–131.

Su, I.H., Dobenecker, M.W., Dickinson, E., Oser, M., Basavaraj, A., Marqueron, R., Viale, A., Reinberg, D., Wülfing, C., and Tarakhovsky, A. (2005). Polycomb group protein ezh2 controls actin polymerization and cell signaling. Cell *121*, 425–436.

Suh, J., and Rabson, A.B. (2004). NF-kappaB activation in human prostate cancer: important mediator or epiphenomenon? J. Cell. Biochem. *91*, 100–117.

Thu, Y.M., and Richmond, A. (2010). NF-κB inducing kinase: a key regulator in the immune system and in cancer. Cytokine Growth Factor Rev. *21*, 213–226.

Trabucchi, M., Briata, P., Garcia-Mayoral, M., Haase, A.D., Filipowicz, W., Ramos, A., Gherzi, R., and Rosenfeld, M.G. (2009). The RNA-binding protein KSRP promotes the biogenesis of a subset of microRNAs. Nature *459*, 1010–1014.

Valastyan, S., Reinhardt, F., Benaich, N., Calogrias, D., Szász, A.M., Wang, Z.C., Brock, J.E., Richardson, A.L., and Weinberg, R.A. (2009). A pleiotropically acting microRNA, miR-31, inhibits breast cancer metastasis. Cell *137*, 1032–1046.

Varambally, S., Dhanasekaran, S.M., Zhou, M., Barrette, T.R., Kumar-Sinha, C., Sanda, M.G., Ghosh, D., Pienta, K.J., Sewalt, R.G., Otte, A.P., et al. (2002). The polycomb group protein EZH2 is involved in progression of prostate cancer. Nature *419*, 624–629.

Varambally, S., Cao, Q., Mani, R.S., Shankar, S., Wang, X., Ateeq, B., Laxman, B., Cao, X., Jing, X., Ramnarayanan, K., et al. (2008). Genomic loss of microRNA-101 leads to overexpression of histone methyltransferase EZH2 in cancer. Science *322*, 1695–1699.

Ventura, A., and Jacks, T. (2009). MicroRNAs and cancer: short RNAs go a long way. Cell *136*, 586–591.

Watanabe, M., Ohsugi, T., Shoda, M., Ishida, T., Aizawa, S., Maruyama-Nagai, M., Utsunomiya, A., Koga, S., Yamada, Y., Kamihira, S., et al. (2005). Dual targeting of transformed and untransformed HTLV-1-infected T cells by DHMEQ, a potent and selective inhibitor of NF-kappaB, as a strategy for chemoprevention and therapy of adult T-cell leukemia. Blood *106*, 2462–2471.

Yamagishi, M., Ishida, T., Miyake, A., Cooper, D.A., Kelleher, A.D., Suzuki, K., and Watanabe, T. (2009). Retroviral delivery of promoter-targeted shRNA induces long-term silencing of HIV-1 transcription. Microbes Infect. *11*, 500–508.

Yamaguchi, K., and Watanabe, T. (2002). Human T lymphotropic virus type-I and adult T-cell leukemia in Japan. Int. J. Hematol. *76* (*Suppl 2*), 240–245.

Yeung, M.L., Yasunaga, J., Bennasser, Y., Dusetti, N., Harris, D., Ahmad, N., Matsuoka, M., and Jeang, K.T. (2008). Roles for microRNAs, miR-93 and miR-130b, and tumor protein 53-induced nuclear protein 1 tumor suppressor in cell growth dysregulation by human T-cell lymphotrophic virus 1. Cancer Res. *68*, 8976–8985.

Zarnegar, B.J., Wang, Y., Mahoney, D.J., Dempsey, P.W., Cheung, H.H., He, J., Shiba, T., Yang, X., Yeh, W.C., Mak, T.W., et al. (2008a). Noncanonical NF-kappaB activation requires coordinated assembly of a regulatory complex of the adaptors cIAP1, cIAP2, TRAF2 and TRAF3 and the kinase NIK. Nat. Immunol. *9*, 1371–1378.

Zarnegar, B.J., Yamazaki, S., He, J.Q., and Cheng, G. (2008b). Control of canonical NF-kappaB activation through the NIK-IKK complex pathway. Proc. Natl. Acad. Sci. USA *105*, 3503–3508.

Genes to Cells

Transcriptional regulation of the *CADM1* gene by retinoic acid during the neural differentiation of murine embryonal carcinoma P19 cells

Takeshi Ito, Yuko Williams-Nate, Miwako Iwai, Yumi Tsuboi, Man Hagiyama, Akihiko Ito, Mika Sakurai-Yageta and Yoshinori Murakami*

Division of Molecular Pathology, Institute of Medical Science, The University of Tokyo, 4-6-1 Shirokanedai, Minato-ku, Tokyo 108-8639, Japan

CADM1 is a multifunctional cell adhesion molecule expressed predominantly in the nerve system, testis and lung. The expression of the *Cadm1* gene is induced during the neural differentiation of murine embryonal carcinoma P19 cells by treatment with retinoic acid (RA). Here, we show that the suppression of CADM1 expression using RNAi interfered with P19 cell aggregation and reduced cell populations expressing MAP2 after RA treatment. Nonaggregated P19 cells were not differentiated into neurons, suggesting that CADM1 participates in the aggregate formation and neuronal differentiation of P19 *in vitro*. A luciferase assay of a series of deletion mutants of the CADM1 promoter localized an RA-responsive *cis*-acting element to an approximately 90-bp fragment upstream of the translational start site. This element contains a putative binding site for transcription factor Sp1, named Sp1-binding site-1 (Sp1BS-1). Sp1BS-1 and adjacent Sp1-binding sites (Sp1BS-2 and Sp1BS-3) showed enhanced transcriptional activity by RA. Moreover, a chromatin immunoprecipitation showed that RA receptor (RAR)α was associated with a DNA fragment containing Sp1BS-1, whereas suppression of RARα expression using siRNA reduced the responsiveness of the CADM1 promoter to RA. These results suggest that Sp1 plays a critical role in RA-induced CADM1 expression through possible interaction with RARα in the neural differentiation of P19.

Introduction

CADM1 is an immunoglobulin superfamily cell adhesion molecule, which is expressed in most neuroepithelial tissues, predominantly in the brain, peripheral nerve, testis and lung (Kuramochi *et al.* 2001; Murakami 2005). Besides the tumor suppressor activity originally reported, CADM1 is shown to be involved in a variety of physiological and pathological phenomena, including synapse formation, spermatogenesis, mast cell interaction and immunological response mediated by natural killer cells, and is previously described as TSLC1/IGSF4/Necl-2/SynCAM1/SgIGSF/RA175 (Wakayama *et al.* 2001; Biederer *et al.* 2002; Ito *et al.* 2003; Boles *et al.* 2005; Takai *et al.* 2008). In the nerve system, CADM1 acts as a presynaptic and a postsynaptic adhesion molecule and plays an essential role in synapse formation (Biederer *et al.* 2002). However, loss of CADM1 expression provides a significant marker of more malignant types of neuroblastomas (Ando *et al.* 2008; Michels *et al.* 2008; Nowacki *et al.* 2008). Furthermore, it has been reported that the expression of mouse *Cadm1* is enhanced during neural differentiation of murine embryonal carcinoma cells, P19, induced by retinoic acid (RA) (Urase *et al.* 2001). These findings suggest that CADM1 plays an important role in neural differentiation as a downstream effecter of RA. Little is known, however, as to the role of CADM1 in the neural differentiation of P19 cells as well as the precise mechanism of the *CADM1* gene expression induced by RA.

P19 cells were originally established from a teratocarcinoma in C3H/HE mice and have the potential to differentiate into derivatives of all three germ layers (McBurney 1993). Treatment of P19 cell aggregates

Communicated by: Hideyuki Saya
**Correspondence*: ymurakam@ims.u-tokyo.ac.jp

DOI: 10.1111/j.1365-2443.2011.01525.x

with RA is known to induce differentiated neurons and glial cells, providing a useful tool to analyze the molecular mechanisms underlying nerve differentiation (Jones-Villeneuve *et al.* 1982). RA, the most active form of vitamin A, is an important molecule for regulating the differentiation, proliferation, and apoptosis of various cells (Ross *et al.* 2000). RA is also an established drug for the treatment of acute promyelocytic leukemia and a compound for the chemoprevention of hepatocellular carcinomas (Flynn *et al.* 1983; Muto *et al.* 1999). The many functions of RA are mediated by its transcriptional regulation of a variety of genes through binding with the nuclear receptor of two distinct families, RA receptors (RARs) and retinoid X receptors (RXRs) (Mangelsdorf & Evans 1995; Chambon 1996).

Neural differentiation of P19 cells by RA accompanies serial expression of various kinds of genes. Three distinct phases are recognized in terms of gene expression induced by RA: the initial primary response phase (0–16 h after RA treatment), the neural differentiation phase (16 h to 2 days after RA treatment) and the terminal differentiation phase (5–6 days after RA treatment) (Soprano *et al.* 2007). A previous report suggests that the CADM1 expression is induced in the neuronal differentiation phase. Therefore, CADM1 appears to be not a direct transcriptional target of RA but, rather, a secondary responsive gene that requires protein synthesis in the initial primary response phase. In fact, no RA-responsive element is present in the *CADM1* gene promoter, suggesting that some additional molecules play a key role in RA-induced CADM1 expression.

In the present study, we investigate the role of CADM1 in the neural differentiation of P19 cells by inhibiting the expression of CADM1 using RNAi and show that the repression of CADM1 reduces the neuronal differentiation by interfering with cell aggregation. Then, we identify *cis*-acting elements containing a putative Sp1-binding site (guanine/cytosine (GC) box) on the CADM1 promoter and show that Sp1 binds to the GC box and that RARα also interacts with the same DNA fragment. These results suggest that RA-induced expression of CADM1, mediated by Sp1, promotes aggregate formation of P19 cells and neuronal differentiation *in vitro*.

Results

Cadm1 expression in P19 cells was enhanced by all-*trans* RA (ATRA)

A previous study reported that the expression of the *Cadm1* gene is up-regulated during the differentiation of P19 cells into neural cells (Urase *et al.* 2001). To clarify the time course of the *Cadm1* gene expression in P19 cells, real-time quantitative PCR was carried out after the exposure of aggregated P19 cells to 1 μM of ATRA for 12–72 h. A maximal level of *Cadm1* mRNA expression of approximately threefold increase was detected at 48 h after exposure to ATRA (Fig. 1A). The amount of CADM1 protein also significantly increased in P19 cells at 48 and 72 h after treatment with ATRA (Fig. 1B and Fig. S1 in Supporting Information).

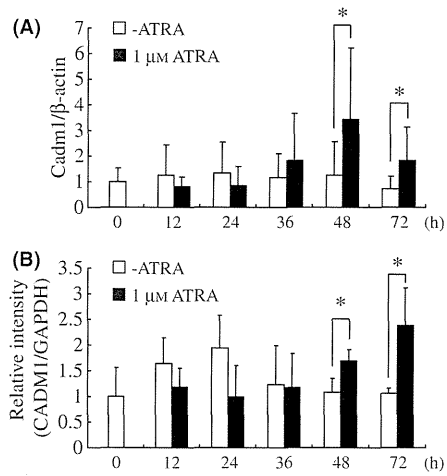

Figure 1 ATRA up-regulates Cadm1 expression. P19 cells were incubated in the aggregated form with or without 1 μM of ATRA for the indicated time. (A) Cadm1 mRNA was quantified by real-time PCR. The results are the means ± SD for six independent experiments. The asterisks indicate statistical significance with $P < 0.05$ as determined by the Student's *t* test. (B) CADM1 protein was quantified by Western blotting using an anti-CADM1 antibody. Each bar is the relative band intensity of CADM1, which was normalized by the band intensity of GAPDH. Error bars are the means ± SD for three independent experiments. The asterisks indicate statistical significance with $P < 0.05$ as determined by the Student's *t* test. ATRA, all-*trans* retinoic acid.

Knockdown of CADM1 interferes with the neuronal differentiation of P19 cells

To elucidate the biological significance of CADM1 in the neural differentiation of P19 cells, we knocked down CADM1 by stably transfecting a vector expressing shRNA against CADM1 into P19 cells (Fig. 2A). Whereas P19 cells transfected with a control vector formed floating aggregates after ATRA treatment, P19 cells transfected with an expression vector of shRNA

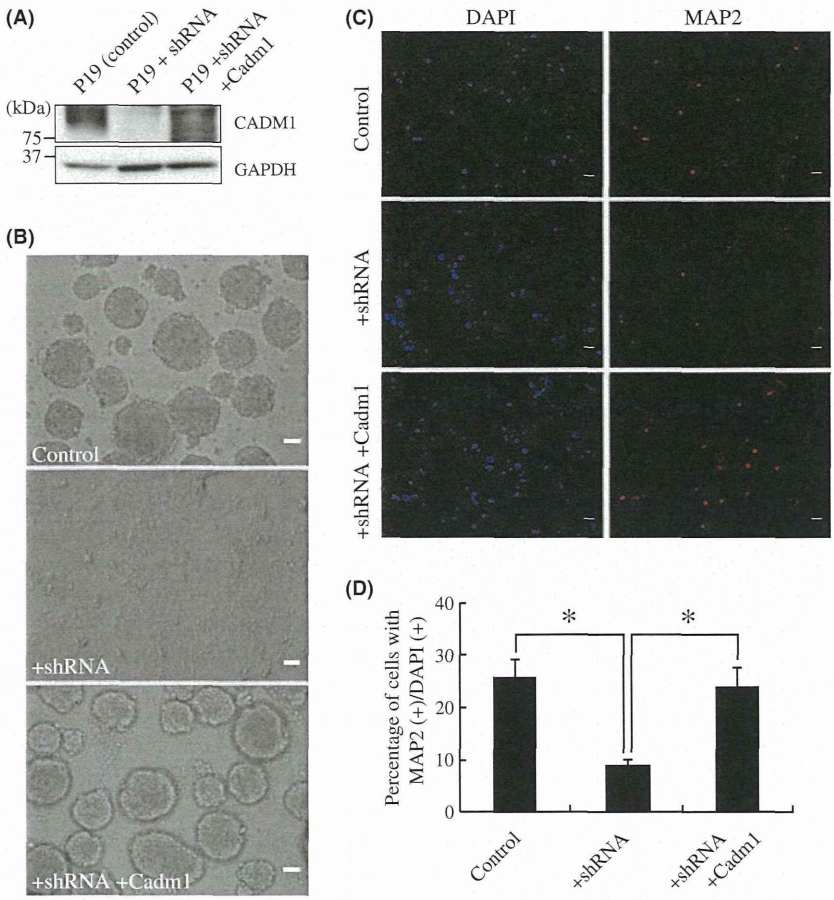

Figure 2 *Interference with neuronal differentiation of P19 cells by knocking down the expression of Cadm1.* (A) Suppression of CADM1 expression in P19 cells and its restoration. P19 cells were stably transfected with a shRNA-expressing vector against CADM1 (P19 + shRNA) or with a control vector (control). P19 + shRNA cells were then transiently transfected with a Cadm1-expressing vector to obtain the P19 + shRNA + Cadm1 cells. The CADM1 protein was detected by Western blotting using an anti-CADM1 antibody. (B) Suppression of CADM1 interferes with the aggregate formation of P19 cells. After incubating on a bacterial plate in the presence of all-*trans* retinoic acid (ATRA) for 4 days, P19 + vector cells formed a large number of floating aggregates, whereas P19 + shRNA cells did not form aggregates but grew as attached cells. Most of P19 + shRNA + Cadm1 cells formed aggregations although a subset of the cells attached to the plates. Bars represent 50 μm. (C) Immunocytochemistry of P19 cells. After incubating on a bacterial plate with ATRA for 4 days, P19 cells were cultured on poly-L-lysine-coated coverslips for 2 days without ATRA and subjected to immunocytochemistry using an anti-MAP2 antibody (red) as well as DAPI (violet). Bars represent 50 μm. (D) Reduction in MAP2-expressing P19 cells by a shRNA against CADM1 and its restoration by a CADM1-expressing vector after treatment with ATRA. Approximately 500 cells (10 scope fields) for each coverslip were counted in terms of MAP2 expression. The percentage of cells with $MAP2^{+}/DAPI^{+}$ is shown. Error bars indicate the means ± SD of three independent experiments. The asterisk indicates statistical significance with $P < 0.05$ as determined by the Student's *t* test.

against CADM1 did not form aggregates but grew as attached cells to a bacterial plate (Fig. 2B). In the RA-induced neural differentiation, P19 cells treated with ATRA were stained with an antibody against MAP2, a neuron-specific marker (Fig. 2C), and the number of MAP2-positive cells was counted. As shown in Fig. 2D, knockdown of CADM1 dramatically reduced the proportion of MAP2-positive cells from 26% to <10%. Similar results were obtained when another sequence of shRNA against CADM1 was transfected into P19 cells (results not shown). Moreover, the aggregated phenotype and the subsequent neuronal differentiation were successfully rescued with the transient transfection of a vector expressing CADM1

(Fig. 2A–D). These results suggest that knockdown of CADM1 interferes with the neuronal differentiation of P19 cells by inhibiting the formation of cell aggregates. Thus, CADM1 is involved in aggregate formation and may promote neuronal differentiation.

RA-responsive elements are in the CADM1 promoter

The functional role of the CADM1 promoter was then examined by a luciferase assay in the presence or absence of ATRA. For this purpose, we constructed a series of deletion mutants from a 2.0-kb sequence (−2004 to −1 bp relative to the translational start site) of the CADM1 promoter and fused them with the *luciferase* gene as a reporter (Fig. 3A). Transient transfection of these constructs into P19 cells showed that RA induced a sevenfold increase in the luciferase activity of the reporter construct carrying the CADM1 promoter [nucleotide (nt) −2004 to −1] when compared with that without RA treatment. A similar degree of RA-induced luciferase activity was observed in a truncated CADM1 promoter of 356 bp (nt −356 to −1). However, luciferase activity induced by RA gradually decreased when the promoter was truncated to shorter fragments of 242, 178 and 112 bp and was finally lost in a fragment of 87 bp (nt −87 to −1), indicating that several DNA sequences located downstream of −356 bp, especially those between −112 and −87 bp, are responsible for transactivation by ATRA. The computer analysis of the CADM1 promoter using the MATCH database (http://www.gene-regulation.com/cgi-bin/pub/programs/match) showed that the region between −112 and −87 bp contains a single GC box, which has been shown to be recognized by specificity protein-1 (Sp1) family proteins. However, no consensus RAR/RXR-binding sequences were detected within this region or within the 2.0-kb CADM1 promoter.

Sp1-binding sites mediate the activation of the CADM1 promoter by ATRA

To elucidate the involvement of the Sp1-binding site located between nucleotides −112 and −87 in the transactivation of the *CADM1* by ATRA, we generated a reporter construct containing triple tandem repeats of the fragment from nucleotide −112 to −70, named as Sp1BS-1. Then, the triple tandem repeat sequences carrying the Sp1-binding site as well as its flanking sequences were fused with the RA-nonresponsive CADM1 promoter from nucleotide −87 to −1 that contains a couple of transcriptional start site (−67 and −62 bp) reported previously (Hori 2010). A construct containing triple tandem repeats of the mutant Sp1BS-1 carrying nucleotide substitutions in the core Sp1-binding sequence from nucleotide −90 to −88 was also generated (Fig. 3B). The triple repeats of wild-type Sp1BS-1 showed markedly increased luciferase activity in comparison with the RA-nonresponsive promoter (nt −87/−1) alone, whereas the triple repeats of mutant Sp1BS-1 lost their activity completely (Fig. 3C). These results indicate that Sp1BS-1 is critical for the activation of the CADM1 promoter by ATRA.

Computer analysis of the promoter identified three additional possible Sp1-binding sites upstream of Sp1BS-1. These sites include Sp1BS-4 from nucleotide −355 to −313, Sp1BS-3 from nucleotide −234 to −191 and Sp1BS-2 from −189 to −146. Therefore, the possible involvement of these Sp1-binding sites was also examined. As shown in Fig. 3C, the luciferase assay of triple tandem repeats of each fragment showed that Sp1BS-2 and Sp1BS-3, but not Sp1BS-4, carried significant transcriptional activity by ATRA, suggesting that Sp1BS-2 and Sp1BS-3 are responsible for RA-induced transactivation of the *CADM1*. In addition, the luciferase activity showed a gradual decrease in a series of deletion mutants, −242/−1, −178/−1 and −112/−1 (Fig. 3A). Furthermore, treatment with mithramycin A, which inhibits Sp1 by masking the GC boxes from binding with Sp1 family proteins, strongly represses RA-induced *CADM1* (Fig. 3D) and the mouse endogenous *Cadm1* (Fig. S2A in Supporting Information) expression, supporting the above findings that Sp1 plays a critical role in the transactivation of *CADM1* by ATRA.

Sp1 and Sp3 bind to the GC box in Sp1BS-1

To identify the transcription factors that bind directly to the GC box in Sp1BS-1, electrophoretic mobility shift assay (EMSA) was carried out using nuclear extracts from P19 cells treated with or without ATRA. As shown in Fig. 4A, three DNA–protein complexes (I, II and III) were identified when a digoxigenin-labeled wild-type Sp1 oligonucleotide probe was used (*lanes 1* and *6*), whereas all three bands completely disappeared when a 1250-fold excess amount of unlabeled wild-type oligonucleotides was included (*lanes 2* and 7). In contrast, these three bands did not disappear when unlabeled mutant oligonucleotides carrying the mutations in the GC box were used, suggesting that these complexes are specific to the sequences in the GC box (*lanes 3* and *8*). Complex I was supershifted

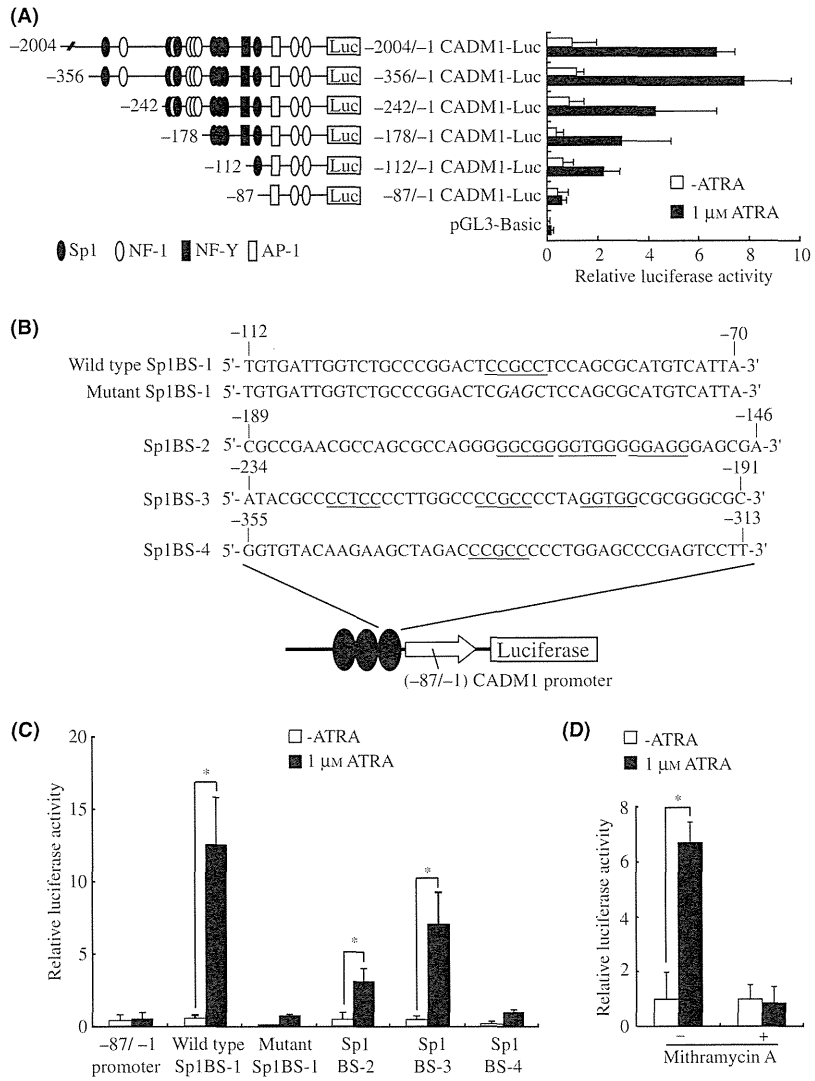

Figure 3 Sp1-binding sites are responsible for the transactivation of the CADM1 promoter induced by all-*trans* retinoic acid (ATRA). (A) The diagram represents putative binding sites of the transcription factors on the CADM1 promoter, and the numbers in the left column represent the location of the 5′ end of each CADM1 promoter fragment relative to the translational start site (defined as +1). A series of deletion constructs of the CADM1 promoter fused to the luciferase reporter was transfected transiently into P19 cells. After incubating with or without 1 μM of ATRA for 48 h, the luciferase activity of each construct was measured and normalized by the Renilla luciferase activity derived from pRL-TK as an internal control. Each value is the mean ± SD of four independent experiments. (B) Schematic diagram and insert sequences of the luciferase reporter plasmids used in the study. The reporter plasmid contains triple tandem repeats of the Sp1-binding sites or its mutant in addition to the retinoic acid (RA)-nonresponsive (−87/−1) CADM1 promoter and the *luciferase* gene. The core Sp1-binding sequences are underlined, and the mutated nucleotides are shown in italics. Sp1BS-1, Sp1BS-2, Sp1BS-3 and Sp1BS-4 are indicated by closed ellipses. (C) Transactivation of the Sp1BS-1, Sp1BS-2, Sp1BS-3 and Sp1BS-4 induced by ATRA. The plasmids containing triple tandem repeats shown in *B* were transfected into P19 cells together with pRL-TK. The cells were cultured with or without ATRA for 48 h. The relative luciferase activity is indicated as the means ± SD of three independent experiments. The asterisks indicate statistical significance with $P < 0.05$ as determined by the Student's *t* test. (D) Mithramycin A blocked the RA-induced transactivation of the *CADM1*. P19 cells were transfected with the reporter plasmid containing the (−2004/−1) CADM1 promoter together with pRL-TK and then incubated with or without 1 μM of ATRA. When specified, 500 nM of mithramycin A was added. Relative luciferase activity is indicated as the means ± SD of three independent experiments. The asterisk indicates statistical significance with $P < 0.05$ as determined by the Student's *t* test.

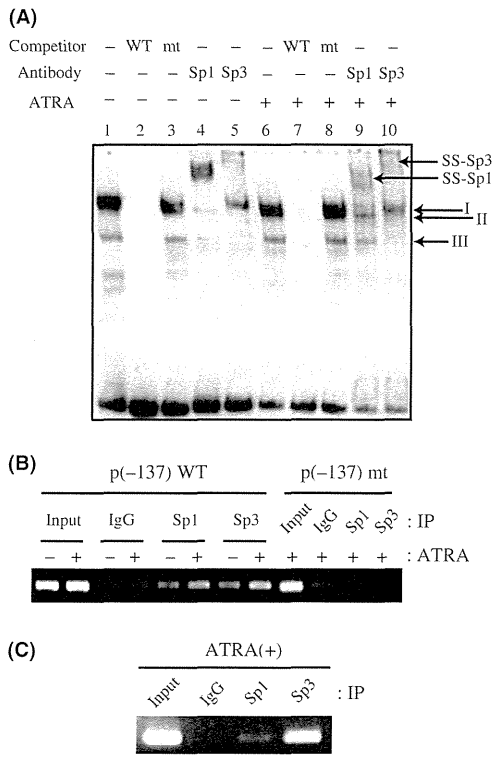

Figure 4 Sp1 and Sp3 bind to Sp1BS-1 on the CADM1 promoter. (A) Electrophoretic mobility shift assay (EMSA) of Sp1BS-1 on the CADM1 promoter. EMSA was carried out using 5 μg of a nuclear extract from P19 cells treated with or without all-*trans* retinoic acid (ATRA) and the DIG-labeled oligonucleotide probe containing a single Sp1 motif in Sp1BS-1 of the CADM1 promoter. Competitive studies were carried out using 1250-fold excess of unlabeled Sp1 probe (*lanes 2* and *7*) or that of a mutated Sp1 probe (*lanes 3* and *8*). Supershift analysis was carried out using antibodies against Sp1 (*lanes 4* and *9*) or Sp3 (*lane 5* and *10*). DNA–protein complexes are indicated by arrows I, II and III. Bands showing supershift by the addition of anti-Sp1 and anti-Sp3 antibodies are indicated by arrows, SS-Sp1 and SS-Sp3, respectively. (B) Chromatin immunoprecipitation (ChIP)-PCR analysis of the Sp1BS-1 on the CADM1 promoter. P19 cells were transfected with (−137/−1) CADM1-luciferase fragment containing a single Sp1 motif (WT) or a mutated Sp1 motif (mt) and treated with or without 1 μM ATRA. Chromatin and associated proteins were extracted and immunoprecipitated with antibodies against Sp1, Sp3 or normal rabbit IgG. The DNA fragment from −116 of the CADM1 promoter to +24 of the *luciferase* gene was amplified by PCR. (C) ChIP-PCR analysis of the endogenous Cadm1 promoter. P19 cells were treated with 1 μM ATRA, and then chromatin and associated proteins were immunoprecipitated with antibodies against Sp1, Sp3 or normal rabbit IgG. The DNA fragment from −283 to +17 of the Cadm1 promoter was then amplified by PCR.

by the addition of the anti-Sp1 antibody, whereas complexes II and III were supershifted by the anti-Sp3 antibody, indicating that both Sp1 and Sp3 bind directly to the Sp1-binding sequence (*lanes 4*, *5*, *9* and *10*). It is noteworthy that, in the series of experiments, the same results were obtained when the nuclear extracts from P19 cells treated with or without ATRA were examined, suggesting that Sp1 and Sp3 binds to Sp1BS-1 even in the absence of ATRA.

To confirm that Sp1 and Sp3 indeed associate with Sp1BS-1 in P19 cells, a chromatin immunoprecipitation (ChIP) assay was carried out in P19 cells transfected with the plasmid containing a 137-bp (nt −137/−1) CADM1 promoter fused with the *luciferase* gene, which included Sp1BS-1 but not other putative Sp1-binding sites on the CADM1 promoter. The association of Sp1 and Sp3 with Sp1BS-1 was shown by PCR of the exogenous DNA fragment of the CADM1 in the presence or absence of ATRA after the immunoprecipitation with anti-Sp1 and anti-Sp3 antibodies, whereas no signal was detected when immunoprecipitated with normal rabbit IgG (Fig. 4B and Fig. S3A in Supporting Information). In contrast, no signals were observed when P19 cells were transfected with the mutant plasmid carrying the mutations in Sp1BS-1, suggesting that Sp1 and Sp3 indeed associate with Sp1BS-1 in P19 cells. The signals from the mouse endogenous Cadm1 promoter were also detected after immunoprecipitation with anti-Sp1 and anti-Sp3 antibodies in the presence of ATRA, suggesting that Sp1 and Sp3 associate with the endogenous Cadm1 promoter (Fig. 4C and Fig. S3B in Supporting Information).

RARα and its coactivator p300 interact with the CADM1 promoter

To identify additional transcription factors that associate with Sp1BS-1 on the CADM1 promoter, a ChIP assay was carried out in P19 cells transfected with the plasmid containing a 2.0-kb (nt −2004/−1) CADM1 promoter fused with the *luciferase* gene. The association of RARα, NF-Y and p300 with Sp1BS-1 was shown by PCR of the exogenous DNA fragment of the *CADM1* after immunoprecipitation with each corresponding antibody, whereas no signal was detected when immunoprecipitated with normal rabbit IgG (Fig. 5A). The signal intensities from the immunoprecipitates by anti-NF-Y or anti-p300 antibodies were enhanced in the presence of ATRA when compared with those in the absence of ATRA. However, the signal intensities from the immunoprecipitates by anti-RARα antibodies were not changed with or

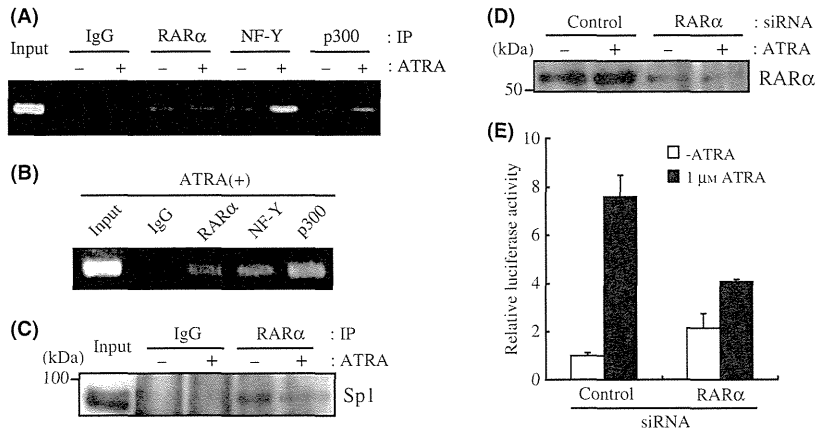

Figure 5 ChIP assay of Sp1BS-1 on the CADM1 promoter. (A) ChIP-PCR analysis of the Sp1BS-1. P19 cells were transfected with (−2004/−1) CADM1-luciferase fragment and treated with or without 1 μM all-*trans* retinoic acid (ATRA), and then chromatin and associated proteins were immunoprecipitated with antibodies against NF-Y, RA receptor (RAR)α and p300 or normal rabbit IgG. The DNA fragment from −116 of the CADM1 promoter to +24 of the *luciferase* gene was then amplified by PCR. (B) ChIP-PCR analysis of the endogenous Cadm1 promoter. P19 cells were treated with 1 μM ATRA, and then chromatin and associated proteins were immunoprecipitated with antibodies against RARα, NF-Y, p300 or normal rabbit IgG. The DNA fragment from −283 to +17 of the Cadm1 promoter was then amplified by PCR. This fragment contains two predicted Sp1-binding sites (one from −182 to −173 and the other from −163 and −154) and two predicted NF-Y-binding sites (one from −240 to −230 and the other from −187 to −177). (C) Co-immunoprecipitation of Sp1 with RARα. Nuclear extract from P19 cells treated with or without 1 μM of ATRA for 48 h was immunoprecipitated with an anti-RARα antibody or IgG and detected by Western blotting using an anti-Sp1 antibody. (D) Suppression of RARα expression using siRNA against RARα was detected by Western blotting. (E) Knockdown of RARα reduced the transactivation activity of the CADM1 promoter by ATRA. P19 cells were co-transfected with siRNA against RARα, (−2004/−1) CADM1-luciferase plasmid, and pRL-TK and incubated in the presence or absence of 1 μM ATRA for 48 h. The relative luciferase activity is indicated as the means ± SD of three independent experiments.

without ATRA treatment (Fig. 5A), supporting the idea that the association of RARα with Sp1BS-1 is independent of ATRA. The signals from the mouse endogenous Cadm1 promoter were also detected after immunoprecipitation with anti-RARα, anti-NF-Y or anti-p300 antibodies in the presence of ATRA, suggesting that these factors indeed associate with the endogenous Cadm1 promoter (Fig. 5B). Furthermore, when P19 cells were treated with or without ATRA and the nuclear extracts were immunoprecipitated with anti-RARα antibody, the bands corresponding to Sp1 were detected with almost equal intensities in both nuclear extracts treated with ATRA and those without ATRA, suggesting again that RARα associates with Sp1 even in the absence of ATRA (Fig. 5C). Finally, knocking down RARα using siRNA abrogated most of the responsiveness of the *CADM1* (Fig. 5D,E) and the mouse endogenous *Cadm1* (Fig. S2B in Supporting Information) to ATRA. Taken together, these findings suggest that RARα, as well as NF-Y and p300, associates with the CADM1 promoter and that the RA-induced activation of the CADM1 promoter is mediated by possible interaction of RARα with Sp1.

Discussion

Earlier studies have reported that the expression of *Cadm1* is induced during the development of the mouse brain and spinal cord. Subsequent studies have shown that CADM1 appears to play an important role in synapse formation, neurite outgrowth and axon guidance (Urase *et al.* 2001; Biederer *et al.* 2002; Hagiyama *et al.* 2009; Niederkofler *et al.* 2010). In this study, we presented an additional role of CADM1 in neural differentiation *in vitro*; CADM1 could promote neuronal differentiation of embryonal carcinoma cells, P19, mediated by RA. It has been reported that two factors are required for neural differentiation of P19 cells, RA stimulation and cell aggregation (Jones-Villeneuve *et al.* 1982; McBurney *et al.* 1982). By knocking down CADM1, P19 cells grew as attached cells on a noncoating bacterial plate without forming aggregation, and subsequently, the proportion of differentiated neuronal cells expressing MAP2 was dramatically reduced. These findings suggest a possible link between the impaired aggregation of P19 cells and the abrogation of the differentiation

program to neuronal cells. Therefore, CADM1 could promote the formation of aggregation and function as a positive regulator of the neuronal differentiation of P19 cells. In this connection, it is suggestive that the neural adhesion molecule, N-cadherin, also promotes the neuronal differentiation of P19 cells (Gao *et al.* 2001). These results suggest that the expression of neural adhesion molecules may play important roles in the neuronal differentiation of P19 cells *in vitro*. Recently, it was reported that germ-line mutations/polymorphisms on the *CADM1* gene were present in a subset of patients with autism spectrum disorder (Zhiling *et al.* 2008). In addition, *Cadm1* knockout mice showed impaired social and emotional behaviors (Takayanagi *et al.* 2010). Our findings *in vitro* might correspond to these disorders *in vivo* and provide a clue to understanding their molecular and cellular mechanisms.

In the latter half of the study, we examined the molecular mechanism of the transcriptional regulation of the *CADM1* gene by RA. By a luciferase assay, we showed that Sp1BS-1, Sp1BS-2 and Sp1BS-3 were involved in the transactivation of the CADM1 promoter by ATRA. Among them, Sp1BS-1 showed the most potent activity in the transactivation of *CADM1* (Fig. 3C). We also showed by ChIP analyses that another transcription factor, NF-Y, could be associated with Sp1BS-1. As NF-Y is known to activate the target genes by forming a complex with adjacent Sp1 (Huang *et al.* 2005), the possible synergistic effect of NF-Y with Sp1 could play a role in the potent activity of Sp1BS-1 in transactivation. However, Sp1BS-4 did not significantly transactivate the reporter gene (Fig. 3C). Shimada *et al.* reported that five continuous purine or pyrimidine bases present at the 3′ of the Sp1-binding core sequences (CCCGCC or its variant) prevented the Sp1 protein from binding to the target sequences (Shimada *et al.* 2001). Because a similar four-pyridine repeat sequence, CCCT, is present at the 3′ of the Sp1-binding core sequence in Sp1BS-4, Sp1 could neither bind to Sp1BS-4 nor activate it. Nonetheless, it is clear that Sp1 is responsible for the transactivation of the *CADM1* gene mediated by RA through Sp1BS-1, Sp1BS-2 and Sp1BS-3. In this connection, it is noteworthy that some recent studies suggested that the Sp1-binding sites also play important roles in the basal transcriptional activity of the *CADM1* gene independently of RA induction, although the Sp1-binding sites responsible for the CADM1 induction reported in these studies are distinct from Sp1BS-1 (Reamon-Buettner & Borlak 2008, Hori 2010).

We also showed by a ChIP assay that additional transcription factors, including RARα, p300 and NF-Y, were associated with Sp1BS-1 and that the association of p300 and NF-Y was enhanced in the presence of ATRA (Fig. 5A). It is also interesting that suppression of RARα not only abrogated the responsiveness to ATRA but also enhanced the basal promoter activity in the absence of ATRA (Fig. 5E). In the absence of RA, the promoter activity is known to be repressed through chromatin condensation induced by the histone deacetylase (HDAC) activity of corepressors accompanied by RARs, whereas, in the presence of RA, the HDAC complex is replaced by coactivators including p300 and chromatin becomes loose as a result of their histone acetyltransferase activity, leading to the transactivation (Bastien & Rochette-Egly 2004). In this case, the absence of RARα would release its corepressors from the CADM1 promoter, leading to the loss of their HDAC activity.

However, distinct from the majority of the target genes by RA, the CADM1 promoter does not contain a RAR-responsive element. In fact, our results showed that RARα interacts with Sp1 and associates with Sp1-binding sites (Fig. 5A–C). However, the interaction between RARα and Sp3 was not detected (results not shown), although Sp1 and Sp3 can bind to Sp1BS-1 (Fig. 4A,B). In general, Sp3 represses the Sp1-mediated transcription when the corresponding promoter contains two or more Sp1 sites (Wierstra 2008). Therefore, Sp3 may play an inhibitory role in the transactivation of *CADM1* because the CADM1 promoter carries several Sp1 sites. Previous studies have reported that RAR regulates gene expression through interaction with Sp1 in the *urokinase* (Suzuki *et al.* 1999), the *HSD17B2* (Cheng *et al.* 2008), the *ID1/ID2* (van Wageningen *et al.* 2008) and the *MAOB* genes (Wu *et al.* 2009). The present study provides an additional example of this type of indirect regulation of transcription by RAR.

Experimental procedures

P19 cell culture and neural differentiation

P19 cells (ATCC, Rockville, MD, USA) were cultured in an α-minimal essential medium (Sigma, St Louis, MO, USA) supplemented with 7.5% bovine calf serum (Thermo Fisher Scientific, Waltham, MA, USA), 2.5% fetal bovine serum (BioWest, Nuaillé, France), and 100 units/mL penicillin and 100 μg/mL streptomycin (Invitrogen, Carlsbad, CA, USA). The cells were maintained at 37 °C in an incubator containing 5% CO_2. To induce neural differentiation, cells were plated to

bacterial-grade 6-well plates (AS ONE, Osaka, Japan) at a density of 2×10^5 cells/well in the presence of 1 μM of ATRA (Sigma). After 4 days of aggregation, cells were trypsinized to single cells and plated to six-well tissue culture plates at a density of 2×10^5 cells/well in the absence of ATRA. The cells were subjected to immunocytochemistry after a 2-day culture.

Antibodies

A rabbit polyclonal antibody against CADM1 (C18) was raised against 18 synthetic polypeptides at the C terminus of CADM1 coupled with keyhole limpet hemocyanin and purified with an affinity column (MBL, Nagoya, Japan). Rabbit polyclonal antibodies against RARα, NF-YA and p300, goat polyclonal antibodies against Sp1 and GAPDH were obtained from Santa Cruz Biotechnology (Santa Cruz, CA, USA). A mouse monoclonal antibody against MAP2 was purchased from Sigma.

Real-time quantitative PCR

Total cellular RNA was extracted using an RNeasy Mini kit (Qiagen, Hilden, Germany) from P19 cells incubated in the presence or absence of ATRA (1 μM) for specified periods. First-strand cDNA was synthesized using a Transcriptor first-strand cDNA synthesis kit (Roche Diagnostics, Basel, Switzerland) according to the manufacturer's protocol. Real-time quantitative PCR was carried out using LightCycler® (Roche Diagnostics) with Universal Probes (Roche Diagnostics) #64 (for β-actin) or #84 (for Cadm1). The PCR cycling was 95 °C for 10 min followed by 55 cycles at 95 °C for 10 sec and 60 °C for 30 s. The sequences of primers were as follows: for the *Cadm1*, sense 5′-ATTCTGGGCCGCTATTTTG-3′ and antisense 5′-TGTCCTCCTTCTGCATTGATT-3′; for the β-*actin*, sense 5′-CTAAGGCCAACCGTGAAAAG-3′ and antisense 5′-ACCAGAGGCATACAGGGACA-3′.

Western blotting

Western blotting was carried out as previously described (Masuda *et al.* 2002). Briefly, cell lysates were prepared from P19 cells using a lysis buffer containing a protease inhibitor mixture (200 μM 4-(2-aminoethyl) benzenesulfonyl fluoride, 10 μM leupeptin, 1 μM pepstatin A). Equal amounts of total protein (20 μg) were fractionated in 7.5% SDS-PAGE, transferred to a polyvinylidene difluoride membrane (Millipore, Bedford, MA, USA) and incubated with an appropriate antibody. The binding of the primary antibody was detected with the ECL™ Western Blotting Detection Reagent (GE Healthcare, Buckinghamshire, UK) using a peroxidase-conjugated secondary antibody (GE Healthcare).

RNA interference

To silence the expression of CADM1, two pairs of oligonucleotides encoding short hairpin RNA (shRNA) were annealed and subcloned into the *Bam*HI/*Hin*dIII site of the p*Silencer*™ 4.1-CMV neo vector (Applied Biosystems, Foster City, CA, USA). The target sequence of shRNA against CADM1 was nucleotides 1408–1426 of CADM1 mRNA. P19 cells were transfected with shRNA-expressing vector using the Lipofectamine™ LTX reagent (Invitrogen) and selected against 0.5 mg/mL of G418 (Invitrogen). Individual clones were evaluated for the knockdown efficiency of CADM1 protein by Western blotting and used for further analyses. For knockdown using a small interference (siRNA) method, a HP GenomeWide siRNA duplex (Qiagen) against RARα and an ON-TARGET plus siCONTROL Non-targeting Pool (Thermo Fisher Scientific) were transfected into P19 cells using the Lipofectamine™ LTX reagent. The target sequence of siRNA against RARα is 5′-AAGCCUUGCUUUGUUUGUCAA-3′.

Immunocytochemistry

P19 cells transfected with shRNA were cultured in 6-well bacterial plates for 4 days and then replated on poly-L-lysine-coated coverslips and cultured for 2 days. The cells were washed twice in PBS (pH 7.2) and fixed with 4% formaldehyde in PBS for 20 min. Fixed cells were then permeabilized with 0.2% Triton X-100 in PBS for 5 min, blocked for 1 h with 2% normal goat serum and 0.2% Triton X-100 in PBS at room temperature and incubated with antibody against MAP2 diluted at 1 : 300 in 2% normal goat serum in PBS at room temperature for 1 h. After washing three times with PBS, the cells received an application of Alexa-568 conjugated secondary antibody (Invitrogen) for 1 h at room temperature and were washed with PBS. The coverslips were mounted with Prolong Gold with DAPI (Invitrogen) on slide glasses and examined with a Biozero BZ-8000 (Keyence, Osaka, Japan).

Plasmid constructs

The DNA sequence of 2004 bp from −2004 to −1 relative to the translational start site of the *CADM*1 gene was amplified by PCR and cloned into the *Sac*I-*Xho*I sites of the pGL3-Basic (Promega, Madison, WI, USA). A series of truncated mutants was constructed in the context of the (−2004/−1) CADM1-luciferase plasmid. The primers used are shown in Table S1 in Supporting Information. The triple tandem repeats of Sp1-binding sites were generated (Table S2 in Supporting Information) and then cloned into the *Eco*RI site upstream of (−87/−1) CADM1 promoter, which was cloned into the *Sac*I-*Xho*I sites of the pGL3-Basic. Cadm1 expression vector was generated by subcloning the mouse Cadm1 coding sequence into *Sal*I site of pBact-STneoB vector, a gift from Dr. Katsuhiko Mikoshiba.

Luciferase assay

For the luciferase assay, P19 cells were plated on 12-well culture plates at a density of 1×10^5 cells/well. After incubating for over 8 h, cells were transfected transiently with 0.45 μg of

the reporter plasmid and 0.05 μg of pRL-TK (Promega) using Lipofectamine™ LTX (Invitrogen). At 4 h after transfection, the medium was replaced, and the cells were incubated for an additional 8 h. The transfected cells were then replated on six-well bacterial plates and treated with or without 1 μM ATRA for 48 h. Cells were harvested, and luciferase reporter activity was measured using a Lumat LB9507 luminometer (Berthold Technologies, Bad Wildbad, Germany). The results of the promoter activities were normalized to pRL-TK using a dual luciferase reporter assay system (Promega). If necessary, mithramycin A (Sigma) was added to a final concentration of 500 nM together with ATRA.

Nuclear extract preparation

P19 cells (1×10^7) were suspended in 400 μL of buffer A [10 mM Hepes-KOH (pH 7.8), 10 mM KCl, 0.1 mM EDTA, 1 mM dithiothreitol, 0.1% NP-40 and a protease inhibitor mixture] and broken down by a vortex. The nuclear pellet was suspended in 100 μL of buffer C [50 mM Hepes-KOH (pH 7.8), 420 mM KCl, 0.1 mM EDTA, 5 mM $MgCl_2$, 2% glycerol, 1 mM DTT and a protease inhibitor mixture] and rotated at 4 °C for 30 min. Nuclear extracts were then collected by centrifugation and stored at −80 °C.

Electrophoretic mobility shift assay

EMSA was carried out using double-strand oligonucleotides that are identical to the 29-bp sequence (nt −105/−77) within the promoter region of the *CADM1* gene containing a GC box (nt −98/−84). The sequences used for the assays were as follows: wild type, 5′-GGTCTGCCCGGACTCCGCCTCC AGCGCAT-3′; mutant, 5′-GGTCTGCCCGGACTCGAGC TCCAGCGCAT-3′. Binding reactions were carried out with 5 μg nuclear extract in a binding buffer [20 mM Hepes-KOH (pH 7.8), 1 mM EDTA, 10 mM $(NH_4)_2SO_4$, 1 mM DTT, 0.2% Tween 20 (w/v), 30 mM KCl, 100 μg/mL poly(dI-dC) and 10 μg/mL poly-L-lysine]. The reaction mixtures were incubated on ice for 15 min followed by the addition of 150 fmol of the DIG-labeled wild-type probe and incubation on ice for another 15 min. The reaction mixtures were then loaded on 4–20% TBE gel (Invitrogen) in 0.5 × TBE. For competition assays, a 1250-fold molar excess of unlabeled oligonucleotides was incubated with the nuclear extracts before the addition of the labeled probe. For supershift analysis, the anti-Sp1 and the anti-Sp3 antibodies were added after the binding reaction, and the mixtures were then incubated on ice for 30 min.

Chromatin immunoprecipitation (ChIP) assay

ChIP assays were carried out using a Chromatin Immunoprecipitation Assay kit (Millipore) following the manufacturer's protocol. P19 cells were transfected with (−2004/−1) CADM1-luciferase plasmids and incubated for 48 h with or without 1 μM of ATRA. The cells were cross-linked with 1% formaldehyde for 10 min at room temperature, and cross-linking was stopped by the addition of glycine to a final concentration of 125 mM. The cells were washed with cold PBS and lysed with an SDS lysis buffer [1% SDS, 10 mM EDTA and 50 mM Tris (pH 8.1)]. Chromatin was sonicated using the Sonifier 150 (Branson, Danbury, CT, USA) to an average DNA length of 200–1000 bp. Insoluble matter was removed by centrifugation for 10 min at 15 000 *g* at 4 °C. The supernatant (50 μL per each sample) was diluted 10-fold in a ChIP dilution buffer [0.01% SDS, 1.1% Triton X-100, 1.2 mM EDTA, 16.7 mM Tris–HCl (pH 8.1), 500 mM NaCl and a protease inhibitor mixture] and precleared with 20 μL of salmon sperm DNA/protein A agarose-50% slurry for 30 min at 4 °C with agitation. Agarose was removed by brief centrifugation, and the supernatant was transferred to siliconized tubes. The precleared chromatin was incubated with 2 μg of primary antibodies (anti-RARα, anti-NF-YA, anti-p300 or normal rabbit IgG) overnight at 4 °C with constant rotation and then incubated with 20 μL salmon sperm DNA/protein A agarose slurry for 1 h at 4 °C with agitation. Protein A agarose/antibody/chromatin complexes were harvested by gentle centrifugation and washed once with a low-salt Immune Complex Buffer [0.1% SDS, 1% Triton X-100, 2 mM EDTA, 20 mM Tris–HCl (pH 8.1) and 150 mM NaCl], once with a high-salt Immune Complex Buffer [0.1% SDS, 1% Triton X-100, 2 mM EDTA, 20 mM Tris–HCl (pH 8.1) and 500 mM NaCl], once with a LiCl immune complex wash buffer [0.25 M LiCl, 1% IGEPAL-CA630, 1% deoxycholic acid (sodium salt), 1 mM EDTA and 10 mM Tris (pH 8.1)] and twice with a Tris-EDTA buffer [10 mM Tris–HCl (pH 8.0) and 1 mM EDTA]. Chromatin–antibody complexes were eluted by 250 μL of elution buffer [1% SDS and 0.1 M $NaHCO_3$] and incubated at room temperature for 15 min with rotation. This elution step was carried out one more time (total volume = 500 μL). Cross-linking was reversed by the addition of 5 M NaCl (0.2 M final concentration) and incubation of the eluted samples for 4 h at 65 °C. Protein was degraded by incubation for 1 h at 45 °C with 10 μL of 0.5 M EDTA, 20 μL of 1 M Tris–HCl (pH 6.5) and 1 μL of 20 mg/mL Proteinase K. DNA was recovered using Wizard® SV gel and PCR clean-up system (Promega). The exogenous CADM1 promoter region was detected by PCR amplification using a pair of primers flanking the Sp1-binding site (sense 5′-GCGCTGTGATTGGTCTG CC-3′ and antisense 5′-CTTTATGTTTTTGGCGTCTTCC-3′) that yielded the predicted 196-bp product. The endogenous Cadm1 promoter region was detected by PCR amplification using a pair of primers flanking the two predicted Sp1-binding sites from −182 to −173 and from −163 and −154 relative to the translational start site (sense 5′-TACGCAACTTGCTCTT ACACG-3′ and antisense 5′-TCATCCTTACCGCTCAT GGT-3′) that yielded the predicted 300-bp product.

Co-immunoprecipitation assay

P19 cells were cultured on bacterial-grade Petri dishes for 48 h, washed with PBS and cross-linked with 1.5 mM

dithiobis[succinimidylpropionate] (DSP; Thermo Fisher Scientific) in PBS at room temperature for 30 min. After washing three times with PBS, a nuclear extract was obtained. The nuclear extract was precleared with protein A-sepharose (GE Healthcare) at 4 °C for 1 h, incubated with antibody against RARα or normal rabbit IgG at 4 °C for 30 min, added with protein A-sepharose and incubated overnight at 4 °C. The immunoprecipitate was rinsed three times with a lysis buffer [50 mM Tris–HCl (pH 7.5), 150 mM NaCl, 1% Triton X-100, 1 mM DTT and a protease inhibitor mixture], suspended in a sample buffer [0.2 M Tris–HCl (pH 6.8), 30% glycerol, 6% SDS, 15% 2-mercaptoethanol, 0.03% bromophenol blue] and incubated at 95 °C for 5 min. The samples were subjected to SDS-polyacrylamide gel electrophoresis followed by Western blotting.

Acknowledgements

The authors express their gratitude to Dr Jun-ichiro Inoue for his generous help with the Lumat LB9507 luminometer and Dr Katsuhiko Mikoshiba for providing pBact-STneoB vector. The authors have declared no conflict of interest. This work was supported by a Grant-in-Aid for Scientific Research (B) [22300336 for Y.M.] and a Grant-in-Aid for Young Scientists (B) [21790309 for M.SY.] from the Ministry of Education, Culture, Sports, Science, and Technology, Japan; a Grant-in-Aid for the Third Term Comprehensive Control Research for Cancer from the Ministry of Health, Labor, and Welfare, Japan (Y.M.); and a Grant for the Promotion of Fundamental Studies in Health Sciences from the National Institute of Biomedical Innovation (ID 05-10 for Y.M.).

References

Ando, K., Ohira, M., Ozaki, T., Nakagawa, A., Akazawa, K., Suenaga, Y., Nakamura, Y., Koda, T., Kamijo, T., Murakami, Y. & Nakagawara, A. (2008) Expression of TSLC1, a candidate tumor suppressor gene mapped to chromosome 11q23, is downregulated in unfavorable neuroblastoma without promoter hypermethylation. *Int. J. Cancer* **123**, 2087–2094.

Bastien, J. & Rochette-Egly, C. (2004) Nuclear retinoid receptors and the transcription of retinoid-target genes. *Gene* **328**, 1–16.

Biederer, T., Sara, Y., Mozhayeva, M., Atasoy, D., Liu, X., Kavalali, E.T. & Sudhof, T.C. (2002) SynCAM, a synaptic adhesion molecule that drives synapse assembly. *Science* **297**, 1525–1531.

Boles, K.S., Barchet, W., Diacovo, T., Cella, M. & Colonna, M. (2005) The tumor suppressor TSLC1/NECL-2 triggers NK-cell and CD8+ T-cell responses through the cell-surface receptor CRTAM. *Blood* **106**, 779–786.

Chambon, P. (1996) A decade of molecular biology of retinoic acid receptors. *FASEB J.* **10**, 940–954.

Cheng, Y.H., Yin, P., Xue, Q., Yilmaz, B., Dawson, M.I. & Bulun, S.E. (2008) Retinoic acid (RA) regulates 17beta-hydroxysteroid dehydrogenase type 2 expression in endometrium: interaction of RA receptors with specificity protein (SP) 1/SP3 for estradiol metabolism. *J. Clin. Endocrinol. Metab.* **93**, 1915–1923.

Flynn, P.J., Miller, W.J., Weisdorf, D.J., Arthur, D.C., Brunning, R. & Branda, R.F. (1983) Retinoic acid treatment of acute promyelocytic leukemia: in vitro and in vivo observations. *Blood* **62**, 1211–1217.

Gao, X., Bian, W., Yang, J., Tang, K., Kitani, H., Atsumi, T. & Jing, N. (2001) A role of N-cadherin in neuronal differentiation of embryonic carcinoma P19 cells. *Biochem. Biophys. Res. Commun.* **284**, 1098–1103.

Hagiyama, M., Ichiyanagi, N., Kimura, K.B., Murakami, Y. & Ito, A. (2009) Expression of a soluble isoform of cell adhesion molecule 1 in the brain and its involvement in directional neurite outgrowth. *Am. J. Pathol.* **174**, 2278–2289.

Hori, R.T. (2010) The minimal tumor suppressor in lung cancer-1 promoter is restrained by an inhibitory region. *Mol. Biol. Rep.* **37**, 1979–1985.

Huang, W., Zhao, S., Ammanamanchi, S., Brattain, M., Venkatasubbarao, K. & Freeman, J.W. (2005) Trichostatin A induces transforming growth factor beta type II receptor promoter activity and acetylation of Sp1 by recruitment of PCAF/p300 to a Sp1.NF-Y complex. *J. Biol. Chem.* **280**, 10047–10054.

Ito, A., Jippo, T., Wakayama, T., Morii, E., Koma, Y., Onda, H., Nojima, H., Iseki, S. & Kitamura, Y. (2003) SgIGSF: a new mast-cell adhesion molecule used for attachment to fibroblasts and transcriptionally regulated by MITF. *Blood* **101**, 2601–2608.

Jones-Villeneuve, E.M., McBurney, M.W., Rogers, K.A. & Kalnins, V.I. (1982) Retinoic acid induces embryonal carcinoma cells to differentiate into neurons and glial cells. *J. Cell Biol.* **94**, 253–262.

Kuramochi, M., Fukuhara, H., Nobukuni, T., Kanbe, T., Maruyama, T., Ghosh, H.P., Pletcher, M., Isomura, M., Onizuka, M., Kitamura, T., Sekiya, T., Reeves, R.H. & Murakami, Y. (2001) TSLC1 is a tumor-suppressor gene in human non-small-cell lung cancer. *Nat. Genet.* **27**, 427–430.

Mangelsdorf, D.J. & Evans, R.M. (1995) The RXR heterodimers and orphan receptors. *Cell* **83**, 841–850.

Masuda, M., Yageta, M., Fukuhara, H., Kuramochi, M., Maruyama, T., Nomoto, A. & Murakami, Y. (2002) The tumor suppressor protein TSLC1 is involved in cell-cell adhesion. *J. Biol. Chem.* **277**, 31014–31019.

McBurney, M.W. (1993) P19 embryonal carcinoma cells. *Int. J. Dev. Biol.* **37**, 135–140.

McBurney, M.W., Jones-Villeneuve, E.M., Edwards, M.K. & Anderson, P.J. (1982) Control of muscle and neuronal differentiation in a cultured embryonal carcinoma cell line. *Nature* **299**, 165–167.

Michels, E., Hoebeeck, J., De Preter, K., Schramm, A., Brichard, B., De Paepe, A., Eggert, A., Laureys, G., Vandesompele, J. & Speleman, F. (2008) CADM1 is a strong neuroblastoma candidate gene that maps within a 3.72 Mb critical region of loss on 11q23. *BMC Cancer* **8**, 173.

Murakami, Y. (2005) Involvement of a cell adhesion molecule, TSLC1/IGSF4, in human oncogenesis. *Cancer Sci.* **96**, 543–552.

Muto, Y., Moriwaki, H. & Saito, A. (1999) Prevention of second primary tumors by an acyclic retinoid in patients with hepatocellular carcinoma. *N. Engl. J. Med.* **340**, 1046–1047.

Niederkofler, V., Baeriswyl, T., Ott, R. & Stoeckli, E.T. (2010) Nectin-like molecules/SynCAMs are required for post-crossing commissural axon guidance. *Development* **137**, 427–435.

Nowacki, S., Skowron, M., Oberthuer, A., Fagin, A., Voth, H., Brors, B., Westermann, F., Eggert, A., Hero, B., Berthold, F. & Fischer, M. (2008) Expression of the tumour suppressor gene CADM1 is associated with favourable outcome and inhibits cell survival in neuroblastoma. *Oncogene* **27**, 3329–3338.

Reamon-Buettner, S.M. & Borlak, J. (2008) Epigenetic silencing of cell adhesion molecule 1 in different cancer progenitor cells of transgenic c-Myc and c-Raf mouse lung tumors. *Cancer Res.* **68**, 7587–7596.

Ross, S.A., McCaffery, P.J., Drager, U.C. & De Luca, L.M. (2000) Retinoids in embryonal development. *Physiol. Rev.* **80**, 1021–1054.

Shimada, J., Suzuki, Y., Kim, S.J., Wang, P.C., Matsumura, M. & Kojima, S. (2001) Transactivation via RAR/RXR-Sp1 interaction: characterization of binding between Sp1 and GC box motif. *Mol. Endocrinol.* **15**, 1677–1692.

Soprano, D.R., Teets, B.W. & Soprano, K.J. (2007) Role of retinoic acid in the differentiation of embryonal carcinoma and embryonic stem cells. *Vitam. Horm.* **75**, 69–95.

Suzuki, Y., Shimada, J., Shudo, K., Matsumura, M., Crippa, M.P. & Kojima, S. (1999) Physical interaction between retinoic acid receptor and Sp1: mechanism for induction of urokinase by retinoic acid. *Blood* **93**, 4264–4276.

Takai, Y., Miyoshi, J., Ikeda, W. & Ogita, H. (2008) Nectins and nectin-like molecules: roles in contact inhibition of cell movement and proliferation. *Nat. Rev. Mol. Cell Biol.* **9**, 603–615.

Takayanagi, Y., Fujita, E., Yu, Z., Yamagata, T., Momoi, M.Y., Momoi, T. & Onaka, T. (2010) Impairment of social and emotional behaviors in Cadm1-knockout mice. *Biochem. Biophys. Res. Commun.* **396**, 703–708.

Urase, K., Soyama, A., Fujita, E. & Momoi, T. (2001) Expression of RA175 mRNA, a new member of the immunoglobulin superfamily, in developing mouse brain. *Neuroreport* **12**, 3217–3221.

van Wageningen, S., Breems-de Ridder, M.C., Nigten, J., Nikoloski, G., Erpelinck- Verschueren, C.A., Lowenberg, B., de Witte, T., Tenen, D.G., van der Reijden, B.A. & Jansen, J.H. (2008) Gene transactivation without direct DNA binding defines a novel gain-of-function for PML-RARalpha. *Blood* **111**, 1634–1643.

Wakayama, T., Ohashi, K., Mizuno, K. & Iseki, S. (2001) Cloning and characterization of a novel mouse immunoglobulin superfamily gene expressed in early spermatogenic cells. *Mol. Reprod. Dev.* **60**, 158–164.

Wierstra, I. (2008) Sp1: emerging roles–beyond constitutive activation of TATA-less housekeeping genes. *Biochem. Biophys. Res. Commun.* **372**, 1–13.

Wu, J.B., Chen, K., Ou, X.M. & Shih, J.C. (2009) Retinoic acid activates monoamine oxidase B promoter in human neuronal cells. *J. Biol. Chem.* **284**, 16723–16735.

Zhiling, Y., Fujita, E., Tanabe, Y., Yamagata, T., Momoi, T. & Momoi, M.Y. (2008) Mutations in the gene encoding CADM1 are associated with autism spectrum disorder. *Biochem. Biophys. Res. Commun.* **377**, 926–929.

Received: 24 June 2010
Accepted: 7 April 2011

Supporting Information/Supplementary material

The following Supporting Information can be found in the online version of the article:

Figure S1 ATRA up-regulates CADM1 protein.

Figure S2 Treatment of mithramycin A or knockdown of RARα reduces ATRA-induced up-regulation of Cadm1 mRNA.

Figure S3 Sequence of the human CADM1 and the mouse Cadm1 promoter.

Table S1 Primers used for PCR to construct deletion mutants

Table S2 Synthesized oligonucleotides corresponding to individual tandem repeats

Additional Supporting Information may be found in the online version of this article.

Please note: Wiley-Blackwell are not responsible for the content or functionality of any supporting materials supplied by the authors. Any queries (other than missing material) should be directed to the corresponding author for the article.

THE JOURNAL OF IMMUNOLOGY

Enhanced Nerve–Mast Cell Interaction by a Neuronal Short Isoform of Cell Adhesion Molecule-1

Man Hagiyama, Tadahide Furuno, Yoichiroh Hosokawa, Takanori Iino, Takeshi Ito, Takao Inoue, Mamoru Nakanishi, Yoshinori Murakami and Akihiko Ito

J Immunol 2011; 186:5983-5992; Prepublished online 11 April 2011;
doi: 10.4049/jimmunol.1002244
http://www.jimmunol.org/content/186/10/5983

The Journal of Immunology is published twice each month by
The American Association of Immunologists, Inc.,
9650 Rockville Pike, Bethesda, MD 20814-3994.

Print ISSN: 0022-1767 Online ISSN: 1550-6606.